INTRINSIC DEGRADATION MECHANISM

IN

TRIS(8-HYDROXYQUINOLATO) ALUMINUM-BASED

ORGANIC LIGHT EMITTING DEVICES

By

Hany M. Aziz, B.Sc., M.Eng.

A Thesis

Submitted to the School of Graduate Studies

In Partial Fulfillment of the Requirements

For the Degree

Doctor of Philosophy

McMaster University

INTRINSIC DEGRADATION IN ORGANIC LIGHT EMITTING DEVICES

DOCTOR OF PHILOSOPHY (1999) **MCMASTER UNIVERSITY**

(Materials Science and Engineering) Hamilton, Ontario

TITLE: Intrinsic Degradation Mechanism in Tris(8-Hydroxyquinolato) Aluminum-Based Organic Light Emitting Devices

AUTHOR: Hany M. Aziz, B.Sc. (The American University in Cairo)
M.Eng. (McMaster University)

SUPERVISORS: Zoran D. Popovic, Adjunct Professor; Gu Xu, Associate Professor

NUMBER OF PAGES: xii, 103

ABSTRACT

Intrinsic degradation, which leads to the long-term decrease in the electroluminescence efficiency, has been a major limitation facing the new technology of organic light emitting devices (OLED). Traditionally, degradation has been speculated to be caused by morphological instability of the organic layers, especially the less stable hole transport layer (HTL), or by the formation of deep traps at the hole-injecting contact. These speculations were based on experimental observations showing that doping the organic layers or introducing a buffer layer at the hole-injecting contact can dramatically improve device stability. However, the real causes of OLED degradation remained uncertain.

In this study, the cause of the long-term degradation of OLEDs based on tris(8-hydroxyquinolato) aluminum (AlQ_3), the most widely used electroluminescent molecule, is investigated. OLEDs with various structures are studied. Results reveal that the injection of holes into the AlQ_3 layer is the dominant factor responsible for device degradation. Cationic AlQ_3 species are found to be unstable and their degradation products are fluorescence quenchers that lower the electroluminescence efficiency of OLEDs.

In view of these findings, the effectiveness of stabilizing agents, such as, doping the HTL, introducing a buffer layer at the hole-injecting contact, or using mixed layers of hole and electron transporting molecules, is explained in terms of their role in slowing down the injection of holes into the AlQ_3, which results in a higher electron density and thus a more rapid electron-hole recombination. Therefore, the lifetime of the unstable cationic AlQ_3 species is reduced leading to a significant decrease in AlQ_3 degradation and consequently increases device stability. Other earlier observations pertaining to OLED degradation are also addressed. The degradation mechanism is further demonstrated on OLEDs with dual-layer HTL made of materials with different ionization potentials. The important features of a theoretical framework to model OLED degradation are also discussed.

ACKNOWLEDGMENTS

I wish to express my deepest gratitude to my supervisor, Dr. Zoran Popovic, for his constant guidance, continuous assistance, and for tireless and endless hours in enlightening arguments and discussions. Zoran, without you, this work would not have been possible. Thank you.

I also wish to express my thanks to Dr. Gu Xu for providing a positive and productive environment for his students, and for his supervision, support, and encouragement throughout my years at McMaster University.

I am grateful to Dr. Adrian Kitai for useful discussions, for his faithful guidance, and for long hours in committee meetings.

I am also thankful to Dr. Brian Ives for important suggestions, for his guidance throughout the committee meetings, and for emphasizing a 'scholarly spirit' in undertaking this study.

I am also grateful to the many people whose assistance made this work possible. To Nan-Xing Hu for his synthesis of the raw materials, to Carl Tripp for his assistance with the infrared spectroscopy, and to Ah-Mee Hor for providing access to a well-equipped lab and to many state-of-the-art equipment.

I am indebted to Hala, my beloved wife. Thank you Hala for your love, encouragement, endurance and support throughout all these years, and for endless hours taken from you and Celine.

Above all, words can not express my gratefulness to my Lord, the Good Shepherd, for His Goodness and Love that follow me all the days of my life. For from Him and through Him and to Him are all things. To Him be the glory for ever and ever.

TABLE OF CONTENTS

LIST OF FIGURES

Figure | Page

CHAPTER 1

Introduction

1.1 General Background

Display devices are an important output of an information system. They play a role of an interface between man and machine. Such machines vary in function and size from hand-held personal systems, such as calculators and watches which need small displays, to TV screens and computer monitors which need bigger and higher resolution screens, to advertising panels which need to be even larger and brighter in order to be visible and readable at a distance. They are used in many military and civilian control systems such as navigation instruments and automated machine controls. Because of their role as an indispensable tool in modern life, display devices are currently supporting a multi-billion dollar industry.

1.1.1 Display Devices:

The commonly used display devices can be classified, according to their operating mechanisms, into four main classes; cathodoluminescent, non-emissive, plasma and electroluminescent displays (Wilson 1983). The most common *cathodoluminescent displays* are the cathode ray tubes (CRTs), which are widely used in TVs and as computer monitors. The mechanism of operation of such devices is based on an electron gun which generates an electron beam that falls on a phosphor screen, leading to light emission. CRTs are by far the most widely used display devices at the present time. However, major disadvantages of these devices is their heavy weight and big size which put limitations on their use especially with the recent trend of portable miniature high-tech devices. In addition, their electron deflection optics makes them unsuitable for large flat panel displays. *Non-emissive displays*, as the name implies, are devices that are inherently incapable of emitting light. Liquid crystal devices, LCDs, are the most common in this class. Their mechanism of operation depends on the fact that they consist of molecular chains that can respond to external electric fields by attaining a structural order. As a result, their light propagation properties are changed, leading to their characteristic opaque/transparent transformation behavior. The operation of such devices is therefore based on the presence of a separate illumination source. LCDs are currently widely used in watches, calculators, lap-top computers, airplane cockpit instrumentation, etc. Although the light weight and compact size are both considered to be their strong assets over the CRTs, LCDs suffer from two important drawbacks: the small viewing angle ($\pm$ 45°), and the limited temperature range (-20 to +50°C). These drawbacks, in addition to their dependence on a separate illumination source, have prevented their use on a wider scale. The operation of *plasma displays* depends on creating an electric discharge in a rarefied gas medium placed between two electrodes across which a high electric field is applied. As a result of the electric field, electrons and ions are accelerated and bombard other gas molecules leading to their excitation or ionization. The excited molecules than relax to the ground state leading to the emission of light. Because of their dependence on an electric discharge in a gas medium, plasma displays essentially require high operating voltages (> 100 volts) and demonstrate low brightness (20-40 cd/m^2). The mechanism of operation of the fourth class of display devices, the *electroluminescent devices,* depends on the radiative relaxation (in the form of visible light) of excitation (excitons) generated by an electrical stimulus. These devices can be classified according to the active material used to produce the light emission into *inorganic devices* and *organic devices.*

Inorganic devices: The operation of these devices depends on one of two types of electroluminescence mechanisms. In the first type, light is produced due to the direct recombination of conduction band electrons and valence band holes that move towards each other by a diffusion process controlled by an externally applied dc electric field. This mechanism occurs in p-n junctions of light emitting diodes (LEDs) used in several electronic applications such as laser diodes, indicator lights, and light sources for optical communications. The electroluminescent material is made of a III-V semiconductor compound that is sometimes doped. Because the diodes must be made of single crystal materials, which are difficult to obtain in sizes exceeding few millimeters, their use has been limited to electronic components like the ones mentioned above. In the second type, the electroluminescence mechanism is based on placing a doped phosphor material, between two dielectric layers onto which two electrodes are deposited from outside. Electrons and holes are generated by means of impact ionization or by quantum mechanical tunneling under the effect of a strong externally applied high ac field (~10^6 V/cm). The recombination of the generated charge carriers then takes place at the dopant sites and leads to light emission. The phosphor material is usually a large band gap material, from the II-VI semiconductor compounds group (e.g.: ZnS). Although such devices can be made in relatively bigger sizes than the first type, their use is limited because of the need for a high ac drive voltage (> 100 V) and because of the difficulty of obtaining blue luminescence.

Organic devices: This is the most recent class of light emitting devices. In the most basic device structure, a thin layer (500-1000 nm) of an organic electroluminescent material is placed between two metal electrodes (figure 1.1). Light is produced due to the recombination of electrons and holes that are injected from the electrodes and transported towards each other under the influence of an applied dc field. Organic light emitting devices can be divided according to the size of the molecules of the organic material into: (1) small molecule devices, commonly called "Organic Light Emitting Devices (OLEDs)", usually with molecular weights in the range of 200-800, and (2) large molecule (polymer) devices, called "Polymeric Light Emitting Devices (PLEDs)", with molecular weights > 10^5. Figure 1.2 shows the molecular structures of both *tris*(8-hydroxyquinolato) aluminum, AlQ_3, the most widely used small molecule organic electroluminescent material, and poly(*p*-phenylene vinylene), PPV, the most widely used polymeric electroluminescent material. The main

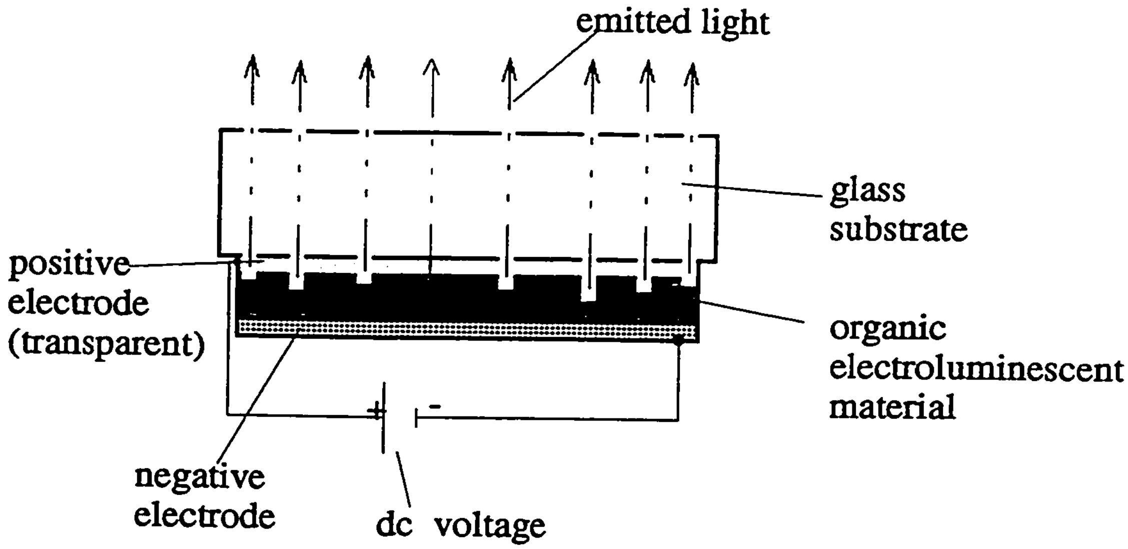

Figure 1.1: Schematic Diagram (side view) of an OLED/PLED

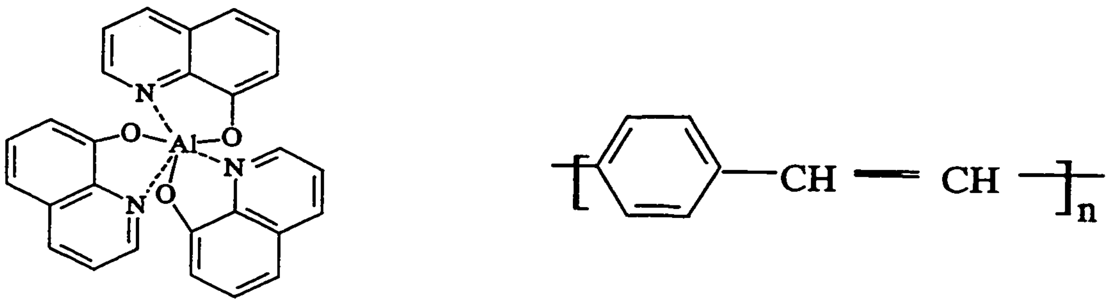

(a) (b)

Figure 1.2: The molecular structure of (a) *tris*(8-hydroxyquinolato) aluminum, AlQ_3, and (b) poly(*p*-phenylene vinylene), PPV.

advantages of these devices include: relatively low operating voltages (< 10 V), high quantum efficiency (~ 1-3 %), versatility of the emission color (from violet to red), unrestricted viewing angle, compact size (< 1 mm, thick) and ease of fabrication. As a result, organic light emitting devices are very competitive candidates for display devices, especially for large-area (> 100 cm^2) flat-panel display applications.

1.1.2 Organic Light Emitting Devices:

Obtaining electroluminescence in an OLED requires placing the organic electroluminescent material between two conducting electrodes with different work functions. Under an applied electric field, the electrode with the lower work function material injects electrons into the conduction band of the organic material, whereas the electrode with the higher work function material injects holes into the valence band of the organic material. The injected electrons and holes are driven, by the electric field, towards each other and recombine to form excited states of e-h (electron-hole) pairs, termed excitons, which then relax radiatively, emitting the excitation energy in the form of optical photons. (figure 1.3) In order for the generated photons to be emitted out of the device at least one of the electrodes must be transparent to visible light, a condition that can not be achieved in materials with low work functions. For this reason, indium-tin-oxide (90% In_2O_3, 10% SnO_2) (ITO), a heavily doped degenerate semiconductor, with a band gap > 3 eV, work function of ~ 4.8-5.0 eV, and transmissivity > 90 % in the visible range, is used as a transparent hole-injecting contact. Because the energy barriers for electron and hole injection at the two electrode/organic material interfaces are different, usually with a higher

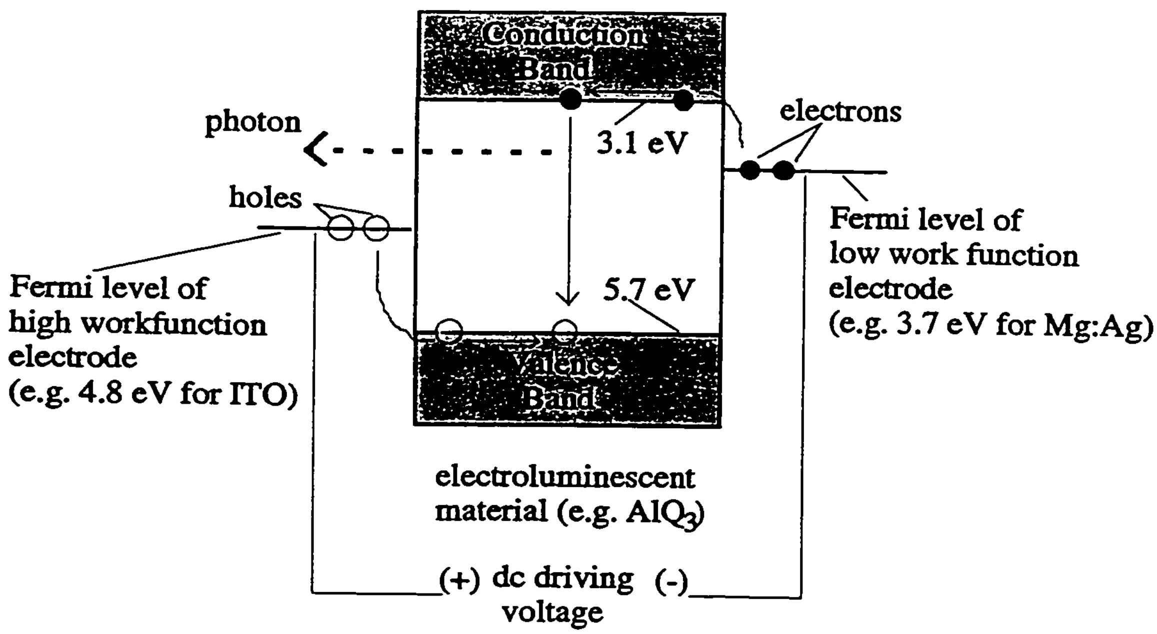

Figure 1.3: Schematic representation of energy bands in a single layer OLED showing charge injection and recombination.

hole injection barrier, (hole injection barrier = energy difference between the Fermi level of the hole-injecting electrode material and the highest state in the valence band of the organic material; electron injection barrier = energy difference between the lowest state in the conduction band of the organic material and the Fermi level of the electron-injecting electrode material), charge injection in single layer OLEDs is generally unbalanced, leading to inefficient electroluminescence. In 1987, the first efficient device based on an organic bilayer structure was reported (Tang and Vanslyke 1987). Since then, OLEDs started to attract the attention, in both academia and industry, because of their potential applications (Sheats *et al.* 1996, Salbeck 1996). In their OLED, Tang and VanSlyke introduced an organic hole transport layer (HTL), in-between the electroluminescent layer and the hole injecting electrode (figure 1.4). Because the ionization potential (energy of the highest valence band states referenced to the vacuum level) of the hole transport material lies between that of the electroluminescent material and the Fermi level of the hole-injecting contact, the injection of holes into the electroluminescent material is facilitated by means of energy cascading. In addition, due to smaller electron affinity (energy of the lowest conduction band state referenced to the vacuum level) of the hole transport material compared to that of the electroluminescent material, the HTL acts as an electron blocking layer, thus reduces the leakage of electrons from the electroluminescent material to the hole-injecting electrode without recombination. As a result, a high external quantum efficiency (0.01 photon/electron), a high luminous efficiency (1.5 lm/W), and a brightness of 1000 cd/m^2 at a low driving voltage (<10 V.) were achieved (Tang and VanSlyke 1987).

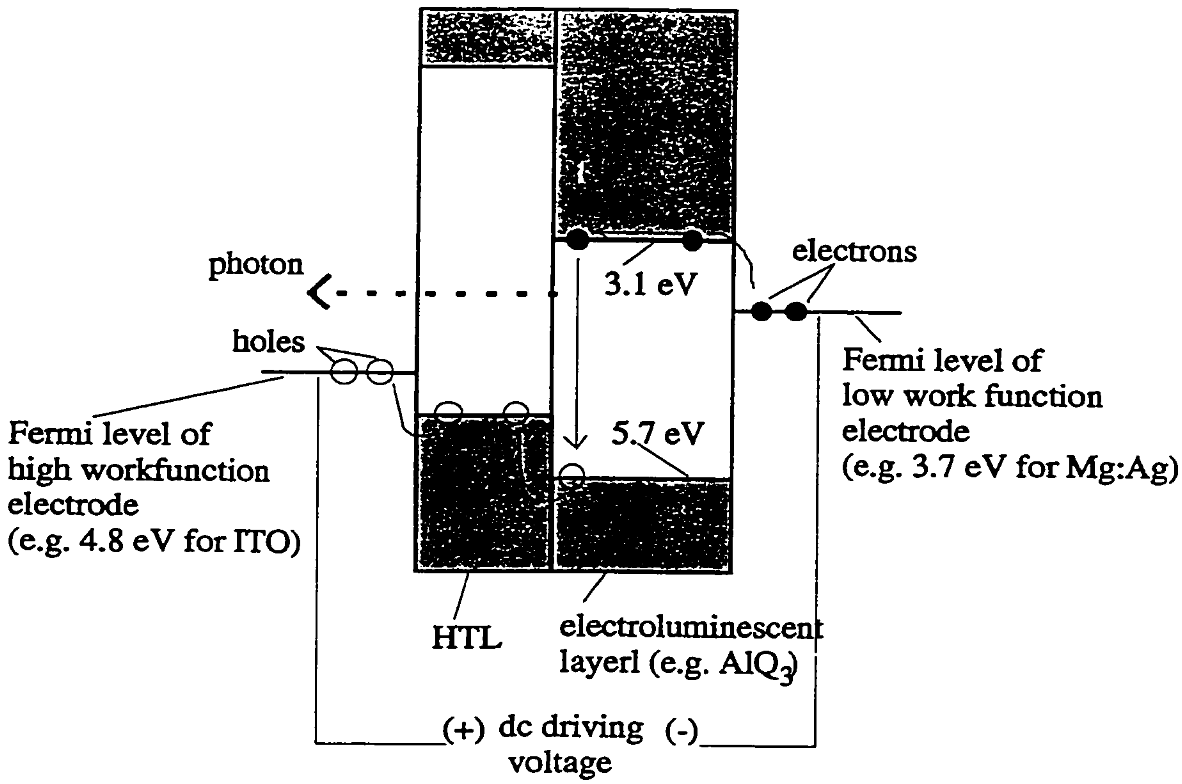

Figure 1.4: Schematic representation of energy bands in a bilayer OLED with a HTL.

Recent advances in the field of organic electroluminescent materials and devices include: (1) synthesizing various materials to obtain luminescence at different wavelengths ranging from red to ultraviolet and demonstrating multi-color and voltage-tunable variable color devices (Shen *et al.* 1997, Sheats *et al.* 1996, Kido *et al.* 1995, Mori *et al.* 1994); and (2) achieving efficient devices with quantum efficiencies and luminescence intensities reaching 7.1% and 140000 cd/m^2, respectively (Kido and Iizumi. 1998, Jabbour *et al.* 1997, Shi and Tang 1997, Wakimoto *et al.* 1997-a).

However, a major problem that has so far prevented the use of OLEDs in any commercial applications is their relatively poor stability. Although storing in ambient conditions is detrimental to the performance of the devices, the short *operating* lifetime is, by far, their major limitation. The average lifetime of an OLED (defined as the time elapsed before the luminance of the OLED decreases to half its initial intensity) usually amounts to few hundred hours (Sheats *et al.* 1996, Salbeck 1996). Although some approaches were found to improve OLEDs stability, and longer lifetimes were reported (Hamada *et al.* 1995, VanSlyke *et al.* 1996, Shi and Tang 1997), the improvement remained limited to few OLED systems with emission colors in the green-yellow range of the visible spectrum.. On the other hand, in order to be suitable for commercial applications, the operating lifetime of OLEDs should exceed 10,000 hours, at an initial luminance intensity of 100 cd/m^2.

1.2 Degradation in OLEDs

1.2.1 Modes of Degradation:

Degradation in OLEDs appears in the form of a gradual decrease of the luminance intensity with time during operation. In general, degradation occurs through the formation of non-emissive "dark" spots, as well as through a long-term "intrinsic" decrease in the electroluminescence efficiency of the devices during operation (McElvain *et al.* 1996). The growth of the non-emissive spots contribute to the decay in the OLED luminance by reducing the operative area of the device, whereas the intrinsic decrease in the electroluminescence efficiency contributes to the decay by gradually decreasing the output luminance intensity of the emitting regions for a constant current input. Several studies focused on dark spot degradation phenomena, and found it to be caused by various humidity-induced mechanisms that lead to: (1) electrode destruction (Burrows *et al.* 1994, Do *et al,* 1994, *ibid.* 1996-a, Aziz and Xu 1996, *ibid.*1997, Kawaharda *et al.* 1997); (2) morphological changes in the electroluminescent layers (Aziz *et al.* 1998-a); or (3) degradation at the electrode/organic layer interface (McElvain *et al.* 1996, Aziz *et al.* 1998-b). Because ambient moisture plays an important role in these mechanisms, dark-spot degradation can be effectively controlled by means of encapsulating the OLEDs in a dry atmosphere (Burrows *et al.* 1994). On the other hand, studies on the intrinsic degradation in OLEDs are relatively few and its causes are still far from being clear or understood.

1.2.2 Review of Earlier Reports on Intrinsic Degradation:

A major suspect of the intrinsic degradation in OLEDs has been the morphological instability of the organic layers, especially the hole transport layer, usually made of organic materials from the diamine group, which is generally characterized by relatively low glass transition temperatures (usually in the range of 60-120 °C) (Shirota *et al.* 1994, Adachi *et al.* 1995, Oktusu *et al.* 1997). Because organic layers in OLEDs are fabricated by vacuum evaporation, the produced layers are in a highly amorphous state, and are thus thermodynamically less favorable than more ordered structures. Due to their high molecular mobility, reflected in the low glass transition temperatures, the layers can undergo morphological changes to attain more stable conformations. A number of studies reported the occurrence of such morphological changes in commonly used hole transport materials (Han *et al.* 1994, *ibid.* 1995-a, *ibid.* 1996), and suggested their role in OLED degradation in terms of causing interlayer delamination, which locally interrupts electrical conduction (Han *et al.* 1995-a) or in terms of providing non-radiative trapping sites (Salbeck 1996). However, these studies were limited to investigating uncovered layers of hole transport materials, and did not include investigations on OLEDs, in which the hole transport layers, being covered by other layers, would be expected to behave differently due to the different nucleation environment of the new morphologies at the surface. An important phenomenon that seemed to support the above view of attributing the intrinsic degradation in OLEDs to the morphological instability of the hole transport layer was reported in 1995 (Hamada *et al.* 1995) in which doping the hole transport layer by a molecular dopant increased the

OLED lifetime by two orders of magnitude. The increased stability was explained in terms of the role of the dopant molecules in preventing the crystallization of the hole transport layer by an entropy effect (Sato and Kanai 1994). As a result, doping the hole transport layer became a widely followed approach to achieve stable OLEDs (Shi and Tang 1997, Sato *et al.* 1997, Wakimoto *et al.* 1997-b, Zhang *et al.* 1998). Moreover, although never detected in OLEDs, morphological instability of the hole transport layer was widely viewed as the dominant degradation agent. In that respect, the faster degradation under OLED operating conditions was attributed to the effect of Joule heating, caused by the current flow, in accelerating these structural changes (Adachi *et al.* 1995, Tessler *et al.* 1998). Therefore, developing new organic hole transport materials with higher glass transition temperature became the focus of many researchers in the field (Shirota *et al.* 1994, *ibid.* 1997, Tanaka *et al.* 1996, Adachi *et al.* 1995, VanSlyke *et al.* 1996, Okutsu *et al.* 1997, Itano *et al.* 1997). With this trend getting stronger, an earlier report that showed no correlation between the OLED lifetime and the glass transition temperature of the hole transport layer passed unnoticed (Adachi *et al.* 1995).

Another degradation mechanism addressing the chemical decomposition of AlQ_3, the most widely used electroluminescent material, was reported in 1996 (Papadimitrakopoulos *et al.* 1996). AlQ_3 was found to react with atmospheric moisture and oxygen, to form a non-emissive polymeric byproduct. However, such mechanism could not account for the intrinsic degradation in encapsulated OLEDs, where the AlQ_3 layer is sealed from the ambient.

VanSlyke *et al.* in 1996, reported that introducing a buffer layer at the hole-injecting contact remarkably improved OLED stability. By inserting a buffer layer of copper phthalocyanine (CuPc) (15 nm thick), they achieved a lifetime of about 3500 hours (at an initial luminance intensity of 510 cd/m^2), from a device with a non-doped hole transport layer. As a result, degradation in OLEDs was attributed to instability at the ITO/HTL that may be attributed to the formation of deep carrier traps which lead to the accumulation of positive space charges in the HTL bulk near the ITO contact. Degradation could also be attributed to degradation of the ITO/HTL interface due to poor adhesion (VanSlyke *et al.* 1996). Since then, introducing a buffer layer at the hole-injecting contact became another widely followed approach to obtain stable OLEDs (Vestweber and Rieb 1997, Zhang *et al.* 1997, Arai *et al.* 1997, Haskal 1997, Sato *et al.* 1997, Wakimoto *et al.* 1997-b).

Other reports attributed degradation (both intrinsic and dark-spot formation) to inter-diffusion between the HTL and the electroluminescent layer (Han *et al.* 1995-b, Do *et al.* 1996-b, Fujihira *et al.* 1996). Apparently, such hypothesis fails to explain the stabilizing effect of introducing a buffer layer at the ITO/HTL interface as discussed above.

Clearly, the causes of the intrinsic degradation in OLEDs have been, at best, speculative, and the underlying mechanisms unknown (Sheats *et al.* 1996). In addition, the effectiveness of the above approaches used in achieving stable OLEDs remained limited to certain OLED material systems. For example, adding a buffer layer at the hole-injecting contact of AlQ_3-based green emitting devices led to lifetimes exceeding 15,000 hours at an initial luminance intensity of 100 cd/m^2 (projected from an accelerated lifetime of 3500 hours at an initial luminance intensity of 510 cd/m^2, according to the widely accepted scaling rule: [initial luminance x half life = constant]) (VanSlyke *et al.* 1996). Adding such layer in distyrylarylene-based blue emitting devices had a little or no effect, and the OLEDs lifetime could only be increased by doping the electroluminescent layer and not the HTL as is usually the case in other OLEDs (Hosokawa *et al.* 1996). Even then, the best lifetime was only 5000 hours at an initial luminance intensity of 100 cd/m^2.

1.3 Research Overview

1.3.1 Research Objective:

The objective of the research work presented in this thesis is to explore and understand the aging phenomena that lead to the long-term intrinsic degradation in OLEDs. It focuses on studying the nature of the fundamental physical and chemical material aging processes that lead to the gradual decrease in the electroluminescence efficiency of the OLEDs during operation. As a scientific research piece of work, it aims at contributing to knowledge. The acquired knowledge is believed to be essential for achieving stable OLEDs (lifetimes > 10,000 hours at an initial luminance intensity of 100 cd/m^2) in two major respects. First, it is necessary for finding effective approaches to hopefully eliminate, or, at least, reduce such aging phenomena, and hence to achieve stable OLEDs with optimum performance of various material systems and emission colors. So, although lifetimes exceeding 10,000 hours have been reported for some green-emitting AlQ_3-based OLED systems, as mentioned above, the employed stabilizing approaches either lead to > 50% higher operating voltages [in case of buffer layers (VanSlyke *et al.* 1996)] or an undesirable change in color [in case of dopants (Hamada *et al.* 1995)], and therefore, alternative stabilizing approaches are still desirable for AlQ_3-based OLEDs. In addition, unveiling the causes of degradation in AlQ_3-based OLEDs will help in understanding the failure processes in other blue and red-emitting OLED systems, due to the fundamental similarities between these systems, and hence in developing stable blue and red-emitting OLEDs. Second, understanding the nature of the aging phenomena is fundamental to developing a theoretical framework that models OLED degradation. Such framework will be important for setting the design rules needed for process-control purposes in the future production of OLEDs on an industrial scale.

1.3.2 Research Approach:

This study is carried on OLEDs based on tris(8-hydroxyquinoline) aluminum (AlQ_3), the most widely used organic small-molecule electroluminescent material. In a controlled experiment approach, various microscopic, spectroscopic and electrical characterization techniques are employed to study both material and device aging phenomena resulting from operating the OLEDs using constant current dc driving conditions. OLEDs fabricated in various structures are investigated, including ones utilizing previously reported stabilizing approaches (e.g. OLEDs with buffer layers at the hole injecting contact, and OLEDs with a doped HTL), and others based on novel structures developed in this study (e.g. OLEDs based on mixed layers of electron and hole transport molecules). From the experimental results of this study, the main cause of intrinsic degradation in OLEDs is elucidated, and used to explain earlier reports on various issues of OLEDs stability. The validity of the proposed degradation mechanism is further verified by demonstrating new approaches to improve OLEDs stability.

1.4 Thesis Outline

This thesis includes seven chapters. Chapter 1, the *Introduction*, was presented above. The outline of the remaining chapters is as follows:

Chapter 2 is an *Overview of OLED Physics.* This chapter is divided into two sections. The first section focuses on the physics of organic electroluminescent materials. In the second section, the operation mechanism of OLEDs is briefly outlined.

Chapter 3, *Experimental Procedures*, presents the details of the experimental methods used in carrying this study. In the first section, sample preparation procedure is presented. In the second section, the methods used in both OLED performance evaluation and material characterization are described.

Chapters 4 and 5 contain a presentation and a discussion of the experimental results acquired throughout this study. In Chapter 4, *Investigation of Various Approaches to Improve OLEDs Stability,* different approaches that increase OLEDs stability are addressed with the purpose of revealing the similarities between them so that the intrinsic degradation mechanism in the devices can be elucidated. The chapter consists of two sections. In the first section, a novel approach, based on introducing a mixed layer of both hole and emitting electron transport molecule, is discussed. The findings revealed by this new approach are used to examine earlier views on the causes of degradation in OLEDs. The second section addresses other approaches previously used to improve OLEDs stability, namely; introducing a buffer layer at the ITO/HTL interface, and doping the HTL. Chapter 5, *The Mechanism of Intrinsic Degradation in AlQ_3-Based OLEDs,* addresses the causes of device degradation. The chapter is divided into four sections. In the first section, the experimental results verifying the postulated degradation mechanism are presented and the underlying process is identified. In the second section, the role of the various approaches in improving OLEDs stability is re-explained in view of the identified degradation mechanism. In the third section, other earlier observations pertaining to OLEDs stability are addressed. In the last section of this chapter, novel approaches to improve OLED stability, based on the new understanding of the degradation mechanism, are demonstrated.

Chapter 6, *Discussion of a Theoretical Framework to Model Degradation in OLEDs*, provides an outline of the important features that must be addressed in developing a theoretical treatment to model OLED degradation. The chapter includes two sections. In the first section, a theoretical framework for calculating OLED degradation rate is proposed. The second section presents a theoretical background for determining the electron and hole concentration profiles that govern OLED degradation.

Finally, Chapter 7, the *Summary and Conclusions*, summarizes the major contributions of this work, and presents the most important conclusions.

CHAPTER 2

Overview of OLED Physics

Before discussing the degradation mechanism in the OLEDs, it seems useful to give a brief overview of the physics of these devices. This chapter is divided into two sections. The first section focuses on the physics of organic electroluminescent materials. In this section, some basic notions on conjugated organic materials will be introduced, followed by an overview of charge-carrier transport processes, and charge-carrier recombination and luminescence phenomena in these materials. In the second section, the operation mechanism of OLEDs is briefly outlined.

2.1 Organic Electroluminescent Materials

2.1.1 Conjugated Organic Materials:

Organic solids are composed of discrete molecules held together by weak intermolecular van der Waals forces; whereas the atoms of a molecule are held together by strong covalent bonds. Because of the weak nature of intermolecular bonding, the properties of the individual molecule are retained in the solid state to a far greater extent than in solids exhibiting other types of bonding. As a result, no study of organic materials can be meaningful without an appreciation of the electronic and optical properties of the individual molecule. It is therefore important to review some of the properties of atomic carbon that are relevant to conjugated aromatic hydrocarbons.

The electronic configuration of a carbon atom in the ground state is $1s^2s^22p^2$, with four electrons in the outer electronic energy level; two paired s electrons and 2 unpaired p electrons. Another possible, but less stable, configuration of the carbon atom occurs by mixing the one 2s and the three 2p orbitals, leading to a set of four orbitals of equal energies (degenerate orbitals), referred to as sp^3 hybrid orbitals. The additional energy required to place the four valence electrons in the tetrahedrally oriented sp^3 orbitals is provided by the energy gained in making four chemical bonds to ligands around the carbon atom. Methane is an example of this type of bonding (Figure 2.1). It is also possible for the s and p orbitals to combine to form three coplanar, 120° apart, sp^2 orbitals (sp^2 hybridization). In this case, one of the three original mutually orthogonal p orbitals, the p_z orbital, remains unaltered. The bonds formed from the three sp^2 orbitals are called σ-bonds. The p_z orbital is perpendicular to the plane of the sp^2 orbitals. The double bonded carbon structure in ethane is an example of this type of bonding (Figure 2.2). In aromatic hydrocarbons, as in the case of organic electroluminescent materials, the p_z orbital of each carbon atom in the benzene ring is perpendicular to the ring plane, and the spacing between the carbon atoms is small enough for overlap between the

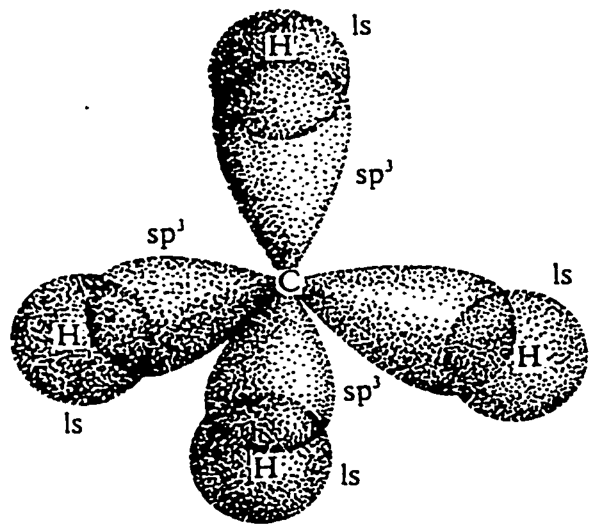

Figure 2.1: sp^3 hybridization in methane (Pope and Swenberg 1982).

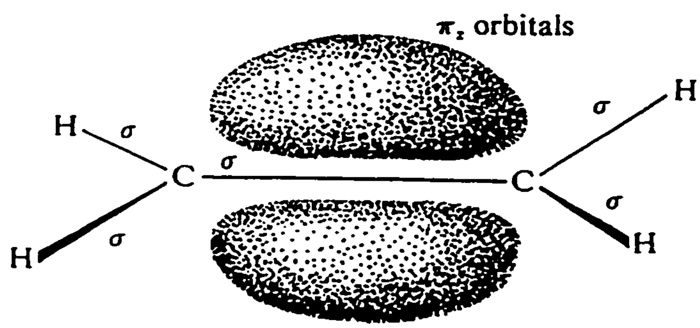

Figure 2.2: sp^2 hybridization and π-orbitals in ethane (Pope and Swenberg 1982).

neighboring p_z orbital to occur. This overlap of the p_z orbitals create what is called π-bonds, characterized by a delocalized electron density above and below the benzene ring. In contrast, the sp^2 orbitals form highly localized electron density bonds in the plane of the ring. The term *conjugated* refers to the characteristic alternation of single and double bonds between the carbon atoms in these molecules. Because the π-electron system of one molecule is highly delocalized, it can also interact with that of another neighboring molecule (Pope and Swenberg 1982). Although such intermolecular interaction can facilitate the transfer of electrons from one molecule to another, leading to macroscopic electronic conduction in the material, its role in amorphous organic solids (the case of OLEDs) is negligible. This is due to the fact that amorphous solids lack a long-range structural order which is necessary for higher spatial packing of the molecules, and hence intermolecular distances that are small enough for strong interactions to occur.

The overlap of the p_z electronic orbitals of the atoms within the individual molecule lies at the crux of the optical properties of conjugated organic materials. This is due to the fact that when two individual atoms are brought into close proximity so that their electronic wave functions overlap, splitting of the outer atomic orbitals into bonding and anti-bonding orbitals must occur according to the Pauli exclusion principle (Cowie 1991) (Figure 2.3). Adding two more atoms to the system will lead to splitting the atomic orbitals into four. With more atoms, there will be more splits in the orbitals into bonding and anti-bonding orbitals, and, as a result, the intervals between each series of orbitals become smaller. This forms two series of closely-spaced orbitals, each of which

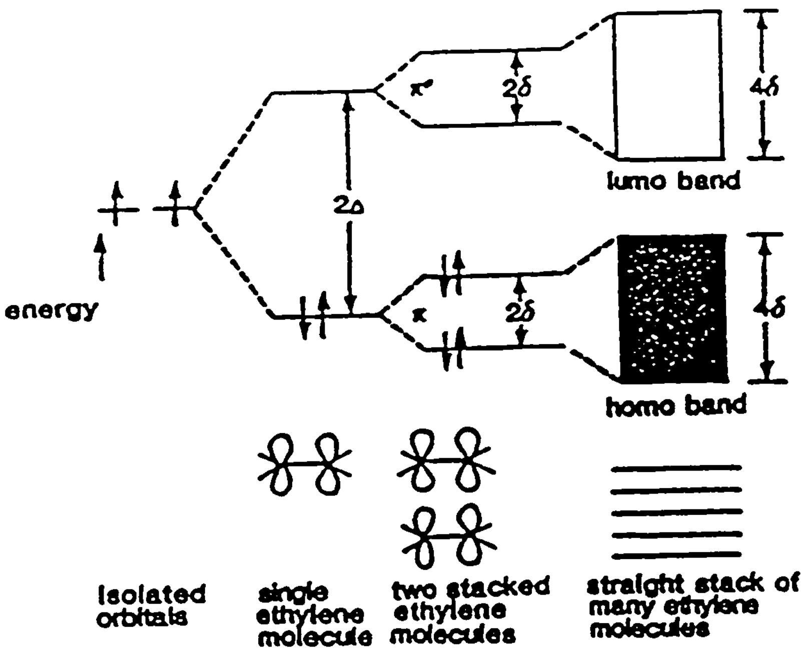

Figure 2.3: The splitting of orbitals and the formation of valence and conduction bands. The dark regions represent energy levels filled with electrons. (Cowie 1991).

can be effectively seen as a continuous band. The two energy bands are separated by a forbidden energy gap. The lower energy band is called the valence band, and consists essentially of occupied orbitals, whereas the higher energy one; the conduction band, consists of mainly unoccupied orbitals. [The probability of occupancy of any orbital in the two bands follows the Fermi-Dirac distribution statistics, and therefore, for any temperature above absolute zero, there is a finite probability that some electrons will have enough energy to be excited from bonding orbitals in the valence band (leaving behind un-occupied orbitals, or *holes*) , and occupy anti-bonding orbitals in the conduction band]. The highest energy orbital in the valence band is called the highest occupied molecular orbital (HOMO), whereas the lowest energy orbital in the conduction band is called the lowest un-occupied molecular orbital (LUMO). Since electronic transitions between the valence and conduction bands of the molecule, require the absorption or the emission of an optical photon, with energy comparable to the forbidden energy gap, the optical properties of the material depend on the height of the gap. For a material to be electroluminescent in the visible range of the electromagnetic spectrum, the energy gap must be in the range of 1.9 eV to 3.1 eV. (The corresponding wavelength of the emitted photon, produced due to an electronic transition from the LUMO to the HOMO, is 650 nm (red color) and 400 nm (violet color), respectively). Generally, stronger overlap between the electronic orbitals (for example, by increasing the delocalized π-electrons, by means of increasing the number of benzene rings in the molecule), leads to more orbital splitting, and therefore results in wider valence and conduction bands, and narrower energy gaps, and vice versa.

2.1.2 Charge-Carrier Transport in Organic Solids

Although the band theory can be used to explain the intramolecular electronic conduction in organic materials, such as along the polymer chains in conjugated polymeric systems, it is not totally suitable to describe the conduction from a macroscopic point of view because of the weak intermolecular interactions. Since macroscopic conduction requires electrons to move from one molecule to another, intermolecular charge transfer is assumed to occur via a hopping mechanism. In contrast to the band model, in which the electrons (or holes) are delocalized throughout the entire solid, and the moving entity is an electron (or a hole) wave, the moving entity, in case of the hopping model, is the 'polaron' (Gutmann and Lyons 1967).

A polaron is an electron (or hole) trapped in a self-induced potential well. Because in a hopping transport case, the time an electron (or hole) spends at a lattice site is much longer than the time it spends during jumping from one site to another (the opposite is true for band model conduction), electron-lattice interactions are strong. This is due to the fact that the residence time of an electron on a lattice site (molecular site) is bigger than the period of intramolecular nuclear vibrations (intramolecular relaxation), the latter being in the order of 10^{-14} s). That means that during the time in which an electron stays at a particular molecular site, the nuclei of the molecule will move to a new equilibrium state with an opposite polarization. This induced polarization of the molecule will act back on the electron itself and reduces its energy, and hence the electron is trapped in a self-induced potential well. The combination of the electron (or hole) and the induced polarization is the polaron (Kao and Hwang 1981).

Because a polaron, by definition, is a charge trapped in a potential energy well, it can not move without first overcoming an energy barrier. So, its movement is essentially a hopping motion. The height of the energy barrier is approximately equal to the sum of the coulombic potential attracting the electron to its self-induced trap and the potential of electron affinity of the originally neutral molecule. These potentials vary smoothly and are better approximated by a triangular barrier (Figure 2.4). Because the energy barrier for an electron in an excited state is lower than that of an electron in the ground state, hopping predominantly occurs via an excited state, and the probability of hopping becomes higher for excited states with longer lifetimes (Kao and Hwang 1981).

Although polaronic effects are important in describing conduction in organic crystals, their role is of secondary importance in amorphous solids. Due to the absence of long-range order in amorphous solids, hopping sites are located in statistically different environments, thus both the site energy and intersite distances are subject to a distribution. Conduction in amorphous solids is therefore primarily described by the energy disorder formalism (Borsenberger and Weiss 1998). The formalism is based on the argument that in the absence of long-range order, the transport manifolds are split into Gaussian distributions of localized states. The hopping site energy distribution arises from disorder-induced fluctuations of dipole-dipole intermolecular potentials resulting from the carrier-induced polarization of the electronic orbitals of surrounding molecules. Due to the weak van der Waals coupling between hopping sites, electronic states of amorphous organic solids are essentially localized. Both the energy and spatial distribution of states can be assumed to have Gaussian distributions because each of them depends on a large number of entities (energy levels or configurational coordinates), each varying randomly by a small amount. Charge transport, therefore, involves hopping to a site which can be of lower or higher energy. Hopping to a lower energy site does not require activation energy and therefore is not enhanced by electric fields, whereas hopping to a site with higher energy, in the absence of thermal activation, requires the assistance of a field. Since applying an external electric field affects the site energy distribution, and reduces the average barrier height for hopping in the field direction, the charge mobility in amorphous organic solids is strongly field-dependent.

2.1.3 Charge-Carrier Recombination and Luminescence in Organic Solids

When an electron and a hole get in close proximity, they recombine, due to coulombic interaction, to form an electron-hole pair called an exciton. In organic molecules, the electron-hole pair is essentially localized on a single molecule (Frenkel exciton), and thus, in effect , forms an excited molecule. Unlike the case of atoms, in which energy states are purely electronic, the energy states of a free molecule include electronic, vibrational, rotational, and translational energy levels. For each electronic level, there is a corresponding manifold of vibrational sublevels. In turn, for each vibrational sublevel there is a manifold of rotational and translational energies. Such energy levels are represented in the form of a

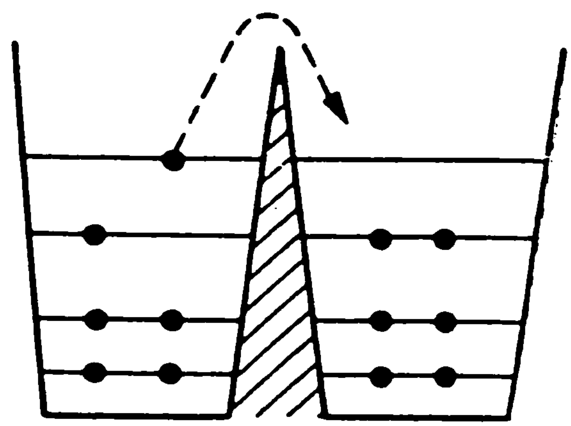

Figure 2.4: Schematic diagram illustrating the hopping of an electron over a potential barrier

Jablonski diagram, in which the electronic levels and the corresponding vibrational sublevels appear as horizontal lines (Figure 2.5). Because the energy spacing of the rotational and transitional levels is very small compared to the spacing between vibrational levels, and also because, in the solid state, the rotational and translational degrees of freedom are essentially blocked, only electronic and vibrational levels are usually shown on the diagram. Each electronic state corresponds to a molecular orbital that can be bonding or anti-bonding. In general, transitions between different electronic states can result in states of same spin multiplicility (electron spin is unchanged during the transition) or states of different spin multiplicity (electron spin is changed during the transition). On the diagram, states with different spin multiplicity are separated horizontally. A state in which the two electrons (according to Pauli exclusion principle, a state is filled by a pair of electrons of opposite spins) have opposite spins is called a singlet state, whereas a state in which the electron pair have parallel spins is called a triplet state (denoted by S_n and T_n, respectively, where n = 0,1,2,.... and refers to the electronic state). The ground state is therefore a singlet state (denoted by S_o). Straight arrows represent radiative transitions (involving the absorption or emission of photons) which can only take place between different electronic states. On the other hand, wavy arrows represent non-radiative transitions (involving the absorption or emission of phonons), which can occur either between different degenerate electronic states (e.g. internal conversion (IC) between states of same spin multiplicity, and intersystem crossing (ISC) between states of different spin multiplicity) or between vibrational sublevels within a particular electronic state (e.g. vibrational relaxation (VR)). (Barltrop and Coyle 1978, Bulovic 1998).

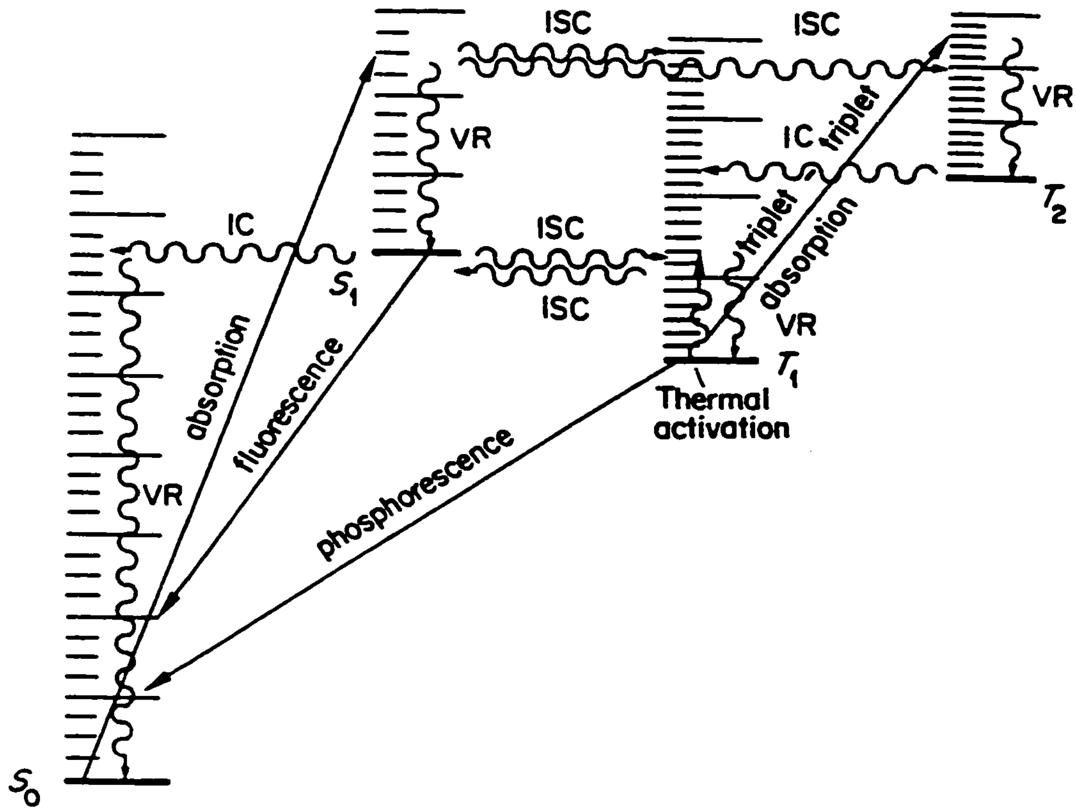

Figure 2.5: Jablonski diagram showing some of the radiative and non-radiative processes in molecules (Barltrop and Coyle 1978).

In general, an electron can be promoted to a higher electronic state of a molecule by photon absorption, dipole-dipole interaction with a neighboring excited molecule (i.e. sensitization), or by being electrically excited, producing, in all cases, a molecule in an excited state. Once in a higher electronic state, the electron tends to relax back to the ground electronic state by losing energy via radiative or non-radiative processes. In a radiative transition, the electron in the higher electronic state loses its energy by emitting a photon and thus produces luminescence. One such case is fluorescence, which is caused by a radiative transition between electronic states of the same spin multiplicity. Another case is phosphorescence, which is caused by a radiative transition between electronic states of different multiplicity. The luminescence intensity depends on the probability of transition and is proportional to the square of the transition moment that embodies the well-known selection rules. Photoluminescence refers to a radiative relaxation (fluorescence or phosphorescence) of an electron from a higher electronic state to which the electron was promoted by means of absorbing a photon. On the other hand, electroluminescence, the central phenomenon in OLEDs, refers to a radiative relaxation of an electron from a higher electronic state that has been generated electrically by the recombination of injected positive and negative charge carriers. Since the various radiative and non-radiative processes compete with each other for the deactivation of the excited state, the relative magnitude of the rate constants of the different processes determines the contribution made by a particular pathway. For example, if an excited state can either fluoresce (rate constant k_f) or undergo non-radiative internal conversion deactivation (rate constant k_{ic}), then the quantum yields of the fluorescence and internal conversion processes (η_f and η_{ic}, respectively) are given by:

$$\eta_f = k_f / (k_f + k_{ic}) \tag{2.1}$$

$$\eta_{ic} = k_{ic} / (k_f + k_{ic}) \tag{2.2}$$

Therefore, if $k_f << k_{ic}$, the population of the excited molecules will be depleted predominantly by the non-radiative route, and the fluorescence will be weak. If, on the other band, k_f and k_{ic} are of the same order, strong fluorescence will be observed (Barltrop and Boyle 1978).

2.2 Operation Mechanism of OLEDs

Light emission in OLEDs is produced by the radiative relaxation of excitons formed by recombination of electrons and holes. Because excitons in organic solids are localized, with electron-hole distances comparable to the size of the molecule, the exciton is essentially an excited molecule; one that has a hole (electron vacancy) in a ground electronic state (i.e. in a valence band state) and an electron in a higher electronic state (i.e. a conduction band state). Because the electron and the hole are not originally created on that molecule (e.g. by absorbing an external photon), but rather injected into it from neighboring molecules, OLEDs operation depends on the direct injection of holes and electrons into the valence and the conduction bands of the electroluminescent material, respectively, from an external source. That requires placing the organic electroluminescent material between two conducting electrodes, one of which must be made of a low work function material, whereas the other must be made of a high work function material. The first serves as an electron-injecting electrode (cathode), where the low work function is necessary to reduce the height of the injection barrier between the cathode Fermi level and the edge of the conduction band (i.e. the LUMO level) of the electroluminescent material. On the other hand, the hole-injecting anode must have a high work function to reduce the height of the injection barrier between the anode Fermi level and the edge of the valence band (i.e. the HOMO level) as shown in figure 1.3 in chapter one of this work. Under a forward bias (defined as an external voltage applied across the two electrodes such that the cathode potential is negative with respect to the anode), electrons are injected from the cathode to the conduction band of the electroluminescent material, and holes are injected from the anode into the valence band. In general, charge injection at a metal/organic interface can proceed by one of two mechanisms: thermionic emission, and quantum mechanical tunneling. Because of the energy mismatch between the Fermi level of the electrode and the HOMO or LUMO of the organic material, both electrode/organic interfaces form blocking (Schottky) barriers. According to the thermionic emission mechanism, charge carriers can cross over the potential energy barrier if they have sufficient energy, and thus shows an Arrhenius behavior. Because the Shottky barrier height is modified by the external electric field, increasing the voltage in a forward bias leads to an exponential increase in the flux of the injected carriers, by means of lowering the potential barrier at the interface. In this case, the current *vs.* voltage relationship shows a field-assisted thermionic injection behavior of the form (Kalinowski 1996-a):

$$I \propto F^{3/4} \exp(\eta F^{1/2}) \tag{2.3}$$

where I represents the current, F the electric field, and η is a temperature dependent parameter.

In the tunneling mechanism, on the other hand, the charge carriers can tunnel through the potential barrier without necessarily having the sufficient energy to go over it. This mechanism is more dominant at high electric fields because of their effect on narrowing the width of the potential barrier, thus leading to more efficient tunneling (Kao and Hwang 1981). Experimentally, the current *vs.* voltage characteristics of OLEDs more closely fit the Fowler-Nordheim tunnel model (Fowler and Nordheim 1928):

$$I \propto F^2 \exp(-\kappa/F) \tag{2.4}$$

where κ is a parameter that depends on the barrier shape. Therefore, tunneling is believed to be the dominant injection mechanism in OLEDs (Scott *et al.* 1997, Kawabe *et al.* 1998).

The injected carriers are then as discussed in section 2.1.2. Driven towards each other by the applied electric field, they recombine and produce excitons, which can then decay radiatively or non-radiatively, as outlined in section 2.1.3. Clearly, the dissipation of exciton energy through non-radiative paths reduces the quantum efficiency (the ratio of emitted photons to injected electrons) of the OLEDs. Some carriers can also reach the opposite electrode before recombining with a counter carrier. This leakage of carriers can be significant in cases of unbalanced electron and hole injection processes as a result of big differences in the hole and electron injection barriers at the two electrodes, leading to poor quantum efficiencies. To reduce this effect, unipolar charge transport layers with HOMO or LUMO levels better matched to the Fermi levels of the electrodes are often placed in-between the electroluminescent material and the electrode as discussed in section 1.1.2 of this work. The presence of the chargc transport layer leads to an easier injection of the desired charge carrier into the electroluminescent layer, and at the same time, blocks the counter charge, thus preventing its leakage from the electroluminescent layer to the electrode.

CHAPTER 3

Experimental Procedures

In this chapter, the details of the experimental procedures and techniques employed in carrying out this study are presented. In the first section, sample preparation procedure is presented. In the second section, the experimental setups used in both OLED performance evaluation and material characterization are described.

3.1 Sample Preparation

The OLEDs are fabricated using physical vapor deposition under vacuum as follows: Square glass substrates (5 cm x 5 cm) are pre-coated with a 55 nm thick layer of indium-tin-oxide, ITO (90% In_2O_3, 10% SnO_2) with a sheet resistance of 10-20 Ω/square, and patterned in the form of ten strips (each about 2 cms long x 5 mm wide), with five strips on each side of the substrate. The ITO strips are coated with a layer of Si_3N_4 (ca. 20 nm thick) that is partially etched above the ten ITO strips to form ten 2mm x 4mm rectangular windows of uncovered ITO, that can function as anodes for ten OLEDs. The ITO and Si_3N_4-patterned substrates are supplied by Xerox Palo Alto Research Center, California, USA. Directly before fabricating the OLEDs, the substrates are cleaned by soaking in an aqueous solution of Decon 75 Concentrate detergent (3% by volume), supplied by BDH Inc., Toronto, Ontario, Canada, for about 20 minutes. After cleaning, the substrates are rinsed by de-ionized water and left to dry in an oven for about 15 minutes at a temperature of 75°C. The substrates are then UV ozone-cleaned in a box equipped with a UV lamp and air for about 20 minutes. The cleaned substrates are then moved to a Process and Vacuum Technology Inc., Ontario, (PVT) vacuum chamber equipped with eight tantalum resistive boats that are used in evaporating the organic materials and the cathode metals. Inside the chamber, the substrate is placed on a stationary holder positioned at about 30 cms above the boats, and equipped with a pneumatic shutter and a manually controlled set of masks that allows the fabrication of up to 5 different OLED structures on the same substrate. In a single pump-down cycle, vacuum in the chamber is achieved by means of an Edwards roughing pump (model 80 Two Stage) and a CTI-Cryogenics high vacuum pump (model CRYO-TORR 8) using a PVT Systems controller (model ACP-2000). The vacuum level is continuously monitored by a Balzers full range ion gauge. The deposition of the organic layers and the cathode on the substrates is carried at a base pressure not exceeding 7×10^{-6} Torr., with the substrates at room temperature. Material evaporation is done by resistive heating of the Ta boats, allowing for the simultaneous evaporation of up to four different materials (from different boats), with the deposition rate of each material on the substrate being monitored by a separate 6 MHz crystal monitor and controlled by a Leybold Inficon IC/5 deposition controller. To fabricate a device, a hole transport layer (HTL) of *N,N'*–di(naphthalene-1-

yl)-*N,N'*-diphenyl-benzidine (NPB) or *N,N'*-diphenyl-*N,N'*-bis(3-methylphenyl)-1,1-biphenyl-4,4'-diamine) (TPD) is first deposited on the substrate at a rate of 0.2-0.4 nm/s. In case of OLEDs with doped HTL, a layer of NPB containing approximately 1 mole % of rubrene (5,6,11,12-tetraphenylnapthacene) is formed by co-evaporation from separate sources at rates of 0.2-0.4 nm/s and 0.002-0.004 nm/s, respectively. Following the deposition of the HTL, the electroluminescent layer, made of tris(8-hydroxyquinolato) aluminum (AlQ_3), an electroluminescent and electron transport molecule, is deposited at a rate of 0.2-0.3 nm/s. In case of OLEDs with a mixed layer, co-evaporation of NPB and AlQ_3 was done at a rate of 0.2-0.6 nm/s each with the individual rate adjusted to obtain various mixing ratios. In OLEDs with a buffer layer at the ITO/HTL interface, a layer of copper phthalocyanine (CuPc) was deposited on the substrate at a rate of 0.1-0.2 nm/s prior to the deposition of the HTL. The thickness of the various organic layers depends on the particular OLED structure, and will be mentioned subsequently in the appropriate sections of this work. From atomic force microscopy measurements, uncertainty in thickness of the different layers is found to be within ±10% of the given values. All organic materials are synthesized, purified and supplied by Xerox Research Centre of Canada. Organic material purification (>99.99% concentration) is done by train sublimation. Figure 3.1 shows the molecular structure of the various organic materials used in making the OLEDs. Following the deposition of the organic layers, a 120 nm thick common cathode is made by co-evaporation of Mg (99.999 %) and Ag (99.999 %) (deposited at 0.9 nm/s: 0.1 nm/s, respectively). The cathode is then covered by an 80 nm thick protective layer of Ag. The metals are supplied by Cerac Speciality Inorganics,

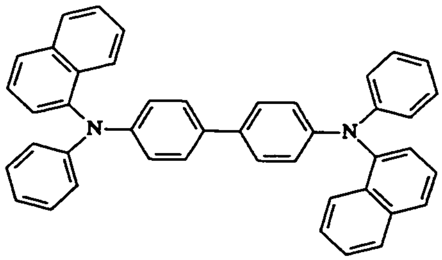

NPB

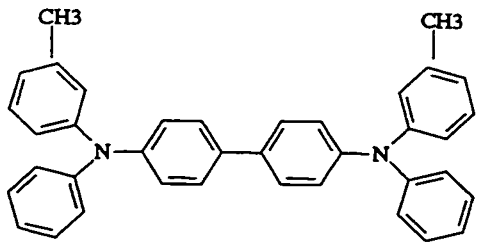

TPD

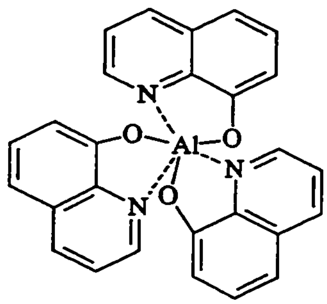

AlQ_3

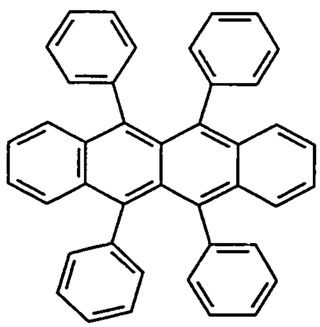

Rubrene

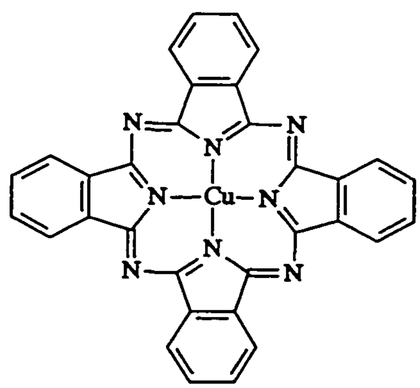

CuPc

Figure 3.1: The molecular structure of the organic materials used in the fabrication of OLEDs studied in this work.

Milwaukee, U.S.A. All layers of the OLED are deposited in the same chamber during the same vacuum cycle.

After completing the OLED fabrication, the vacuum chamber is vented by dry nitrogen. The OLED is then transferred in air and immediately sealed in a box that can be fitted to various experimental setups used in testing the OLEDs. The box is equipped with electrical contacts and is continuously purged by dry nitrogen (<30 ppm moisture) from a Matheson N_2 generator (model 76-94 UHP). The dry atmosphere is necessary to minimize the formation of dark spots due to cathode reaction with ambient moisture (Aziz *et al.* 1998-a, *ibid.* 1998-b).

3.2 Experimental Measurements

3.2.1 OLED Performance Evaluation:

Device performance, defined as the combination of efficiency, lifetime, turn-on voltage and the emission color of an OLED, is evaluated by means of electrical dc measurements. The effect of changing the structure of OLEDs (by means of introducing new layers, changing layer thickness, or doping) on the performance is mainly evaluated by means of : (1) measuring the current density-voltage-luminance (J-V-L) relationship; (2) measuring the lifetime under operating conditions; and (3) obtaining the electroluminescence (EL) spectra of the OLEDs. To follow a controlled experiment approach, the performance of standard devices, fabricated on the same substrates during the same vacuum cycle is evaluated under same conditions. The J-V-L characteristics are obtained using a Keithley 238 Source-Measure unit and a calibrated photodiode, both interfaced to a personal computer. Lifetime measurements are carried out under constant dc current driving conditions using a house-built constant current source and measuring unit that samples the driving voltage and the luminance intensity logarithmically in time domain. The EL spectra are obtained using a Products for Research, Inc. 191933-93 cooled photomultiplier, and an Instruments SA, Inc. DH-20 monochromator for detecting the luminance of the OLED operated under constant current driving conditions. All measurements are carried out at room temperature.

3.2.2 Material Characterization:

The following material thin-film characterization techniques are employed to study aging phenomena in the various OLED layers during device operation:

Optical and Fluorescence Microscopy are used to study morphological changes in the organic layers during device operation. A Leitz Vario-Orthomat microscope and camera system is employed. The system is equipped with a UV illumination, acting as a fluorescence excitation source, and a set of cross polarizers to detect crystalline regions. Aged OLEDs are viewed in a reflective mode (via the glass substrate), or in a transmissive mode (after removing the opaque cathode by means of scotch tape) and compared to fresh (non-aged) ones. Microscopic studies are carried out in air.

Atomic Force Microscopy (AFM) is used to study morphological changes in the organic layer during OLED operation by means of detecting changes in the topography and surface roughness of these layers. A Digital Instruments, Inc. Nanoscope II system is used. The organic layers of aged devices are studied (after removing the cathode) and compared to those of fresh devices. The samples are exposed to air during AFM testing.

Photoluminescence Spectroscopy (PL) is used to study organic material degradation by means of studying changes in the fluorescence quantum efficiency or shifts in the fluorescence peak position. PL spectra are obtained using a Products for Research, Inc. 191933-93 cooled photomultiplier, Oriel Hg-Xe (150W) arc lamp excitation source, and two Instruments SA, Inc. monochromators (DH-10 for illumination and DH-20 for light detection). PL tests are carried out in a dry nitrogen atmosphere at room temperature.

Fourier-Transform Infrared Absorption Spectroscopy (FTIR) is used to study chemical changes in the organic layers (after removing the cathode) by means of detecting degradation byproducts or changes in concentrations of the original chemical species. A Nicolet Magna-IR 550 spectrometer and IR PLAN microscope system, operated in a reflective mode at a lateral resolution of 50 x 50 microns, is used. The samples are exposed to air during testing.

CHAPTER 4

Investigation of Various Approaches to Improve OLEDs Stability

This chapter presents a study on some approaches that lead to an improved OLEDs stability. A novel approach, based on introducing a mixed layer of both hole and emitting electron transport molecule, is presented in the first section. The findings revealed by this new approach are used to examine earlier views on the causes of degradation in OLEDs. The second section presents studies on OLEDs with improved stability based on previously reported approaches, namely; introducing a buffer layer at the ITO/HTL interface, and doping the HTL. Although the last two approaches were reported by other researchers, as previously outlined in section 1.2.2 of this work, they have been studied within the course of this research with a new objective. This objective is to find similarities between the effect of each of these seemingly unrelated approaches, so that the real degradation mechanism in OLEDs can be elucidated. In that respect, the chapter presents new experimental results obtained from OLEDs utilizing novel and previously known stable device structures.

The material contained in this chapter has been published before. The material in the first section has been modified from the original manuscript entitled: "*Improving the Efficiency and Stability of Organic Light Emitting Devices by Using Mixed Emitting Layers*", by: Zoran D. Popovic, Hany Aziz, Carl P. Tripp, Nan-Xing Hu, Ah-Mee Hor, and Gu Xu, published in 1998, in *Proceedings of the SPIE,* Volume 3476, *Organic Light-Emitting Materials and Devices II,* San Diego, CA, July 1998, pp 68-73, where necessary modifications have been made to make it consistent with the general theme of this thesis. The material in the second section has been modified from the original manuscript entitled: "*Degradation Mechanism of Small Molecule-Based Organic Light Emitting Devices*" by: Hany Aziz, Zoran D. Popovic, Nan-Xing Hu, Ah-Mee Hor, and Gu Xu, published in 1999, in *Science,* Volume 283, pp 1900-1902, where necessary modifications have been made to make it consistent with the general theme of this thesis. All the work presented in this chapter; device architecture, sample preparation, set-ups, measurements, analysis of results and the writing were entirely performed and contributed by the author under supervision of Dr. Zoran Popovic. The author acknowledges the contribution of Nan-Xing Hu in the synthesis of the organic raw materials.

4.1 Mixed-Layer OLEDs†

In order to achieve efficient electroluminescence, as discussed earlier in section 2.2, OLEDs are made of separate HTL (made of a hole transport material (HTM), such as, NPB or TPD) and an electroluminescent layer (made of an electroluminescent electron transport material (EETM), such as AlQ_3). Although there have been few attempts to obtain electroluminescence from OLEDs with a single mixed layer, where both the HTM and the EETM are mixed in one layer (Naka *et al.* 1994, Wu *et al.* 1997), or are introduced as guests in an inert host material (Kido *et al.* 1992), such devices were generally less efficient than standard devices made of separate layers of HTM and EETM. In addition, the effect of introducing these mixed layers on the OLEDs stability has not been reported before. Studying the effect of the mixed layer on OLED stability is particularly important to this study because of earlier reports that organic inter-layer diffusion between the HTL and the electroluminescent layer may have a role in device degradation, as mentioned earlier in section 2.2.

4.1.1 Structure of OLEDs with a Mixed Layer:

To simulate a case of inter-diffusion between the HTL and the electroluminescent layer in a standard bilayer OLED, a new device structure is developed. The structure (Figure 4.1a) consists of a mixed layer of NPB and AlQ_3 (ca. 80 nm thick) of various

† Reprinted with permission from [Popovic *et al.*, 1998, *Proceedings of the SPIE*, **3476**, 68].

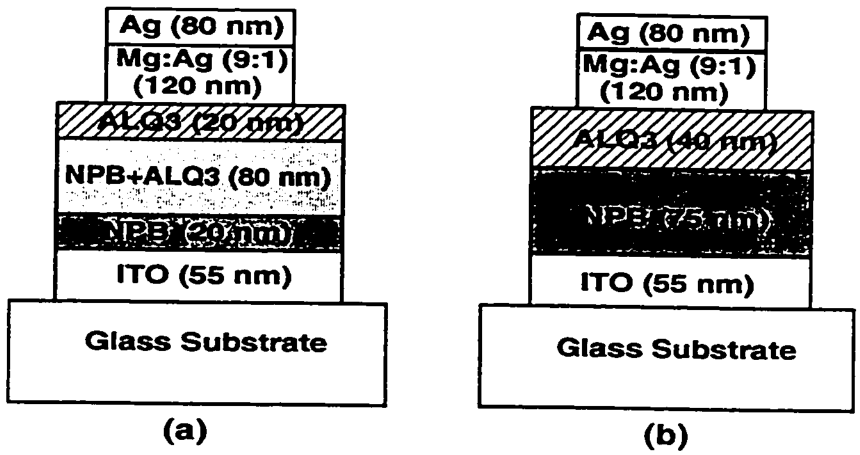

Figure 4.1: (a) Structure of a mixed-layer OLED. (b) Structure of a standard bilayer OLED (Popovic *et al.* 1998).

mixing ratios, serving as a bipolar charge transport and electroluminescent layer, placed between thin layers of pure NPB and AlQ_3 (ca. 20 nm thick each) acting as hole and electron transport layers (HTL and ETL), respectively. The three organic layers are placed between an ITO anode and a Mg:Ag/Ag cathode. Standard bilayer OLEDs (Figure 1b) made from the same materials on the same substrates during the same vacuum cycle are also fabricated to act as references.

4.1.2 Effect of Introducing the Mixed Layer on OLED Performance:

In order to study the effect of introducing the mixed layer on the performance of the OLED, current density-voltage-luminance intensity measurements and lifetime tests are carried out on both the mixed-layer OLEDs and the standard bilayer OLEDs. Figure 4.2 shows the current density *vs.* voltage *(J-V)* and the luminance intensity *vs.* current density *(L-J)* characteristics of a group of mixed-layer OLEDs of various HTM/EETM mixing ratios. The characteristics of a standard bilayer device are also shown for comparison. Apparently, both the turn-on voltage and the EL efficiency (equal to the slope of the L-J linear relationship, and measured in cd/A) depend on the mixing ratio. The highest EL efficiency is ~3.2 cd/A and corresponds to a 50% AlQ_3 -50% NPB weight ratio (~56% AlQ_3 -44% NPB mole ratio). Lower AlQ_3/NPB ratios progressively reduce the turn-on voltage, however, the highest energy conversion efficiency (the output luminous power per unit input electrical power) also corresponds to a 50% AlQ_3 -50% NPB mixed layer and has a value of ~0.6 lm/W (at 100 cd/m^2 luminance). Compared to an EL efficiency of ~2.1 and an energy conversion efficiency of ~ 0.48 lm/W (at 100

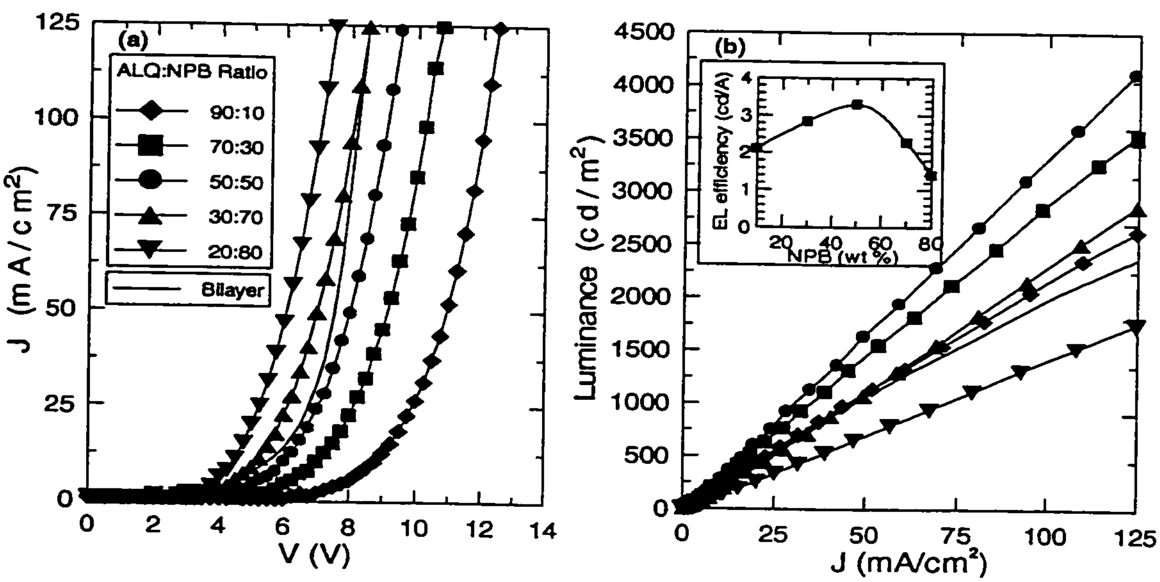

Figure 4.2: (a) Current density *vs.* voltage, and (b) Luminance *vs.* current density characteristics of anode/NPB/ mixed layer/AlQ_3/cathode OLEDs with various AlQ_3/NPB weight ratios in the mixed layers. The characteristics of a standard bilayer OLED are shown for comparison. Inset: EL efficiency *vs.*NPB weight % of the mixed layer. (Popovic *et al.*1998).

cd/m^2 luminance) of a standard bilayer device, an OLED with a 50 % AlQ_3 – 50 % NPB mixed layer has ~ 50 % higher EL efficiency and ~ 25 % higher energy conversion efficiency.

Stability tests show that the operational lifetime of mixed-layer OLEDs is about an order of magnitude longer than that of standard bilayer devices. Compared to a lifetime of only about 45 hours in case of a standard bilayer OLED, a mixed-layer OLED demonstrates a lifetime of about 550 hours (Figure 4.3a). Because the initial luminance of a mixed-layer OLED is higher (770 cd/m^2 compared to 510 cd/m^2 for a standard bilayer OLED), the difference in the lifetimes projected from an initial luminance of 100 cd/m^2 is even bigger. (4250 and 230 hours, respectively, using the scaling rule in section 1.2.2). In addition, the rate of increase of the driving voltage of the devices with mixed layers is found to be much lower than in case of the bilayer devices (Figure 4.3b).

4.1.3 Causes of Higher Efficiency in Mixed-Layer OLEDs:

In an earlier study, we found that OLEDs consisting of a single organic mixed layer without the thin pure NPB and AlQ_3 charge transport layers were less efficient than standard bilayer OLEDs; in agreement with the findings of Naka *et al.* (Naka *et al.* 1994). To investigate the role of these charge transport layers in improving the efficiency, a comparative study involving four different device structures is carried (Figure 4.4). In structure (i), both the HTL and the ETL are present, whereas structures (ii), (iii) and (iv) correspond to OLEDs where the HTL is missing, the ETL is missing,

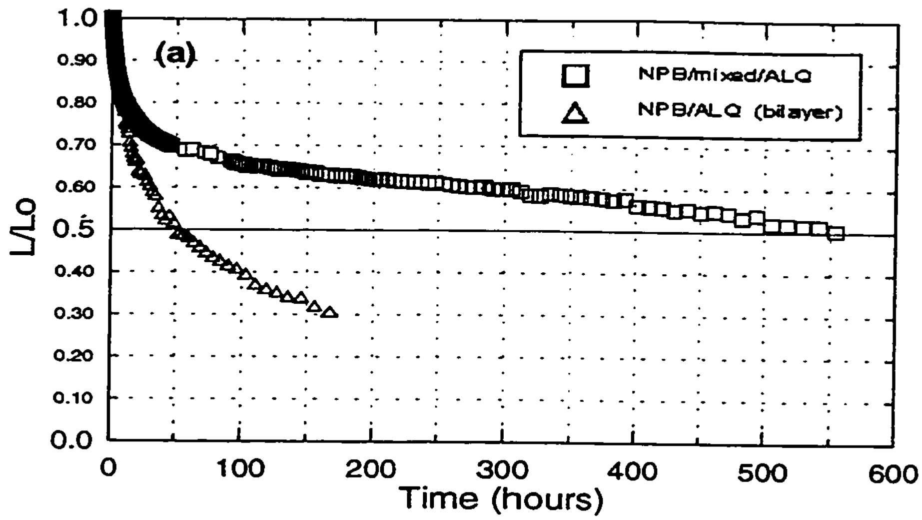

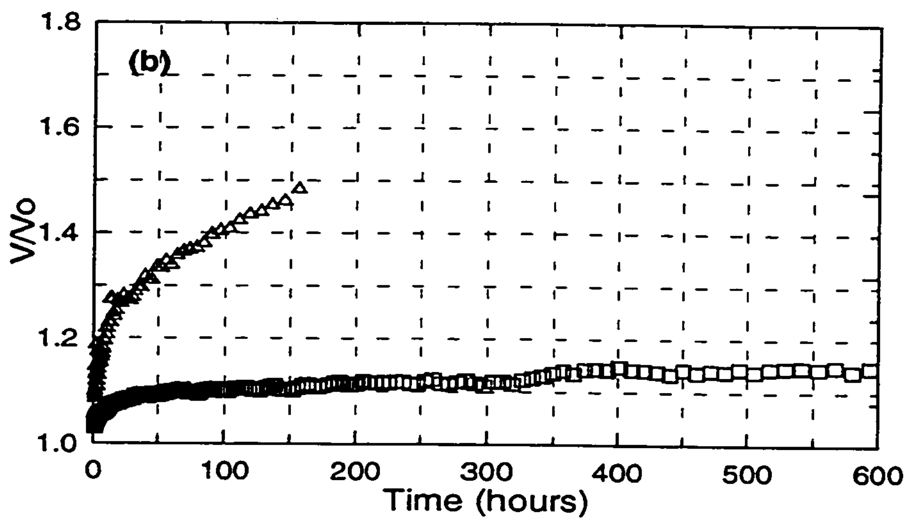

Figure 4.3: (a) Luminance (L)/initial luminance(L_O); and (b) driving voltage (V) / initial driving voltage (V_O) *vs.* time for a mixed-layer OLED and a standard bilayer OLED both stressed at 25mA/cm^2. The initial luminance levels are 770 and 510 cd/m^2, respectively. The initial driving voltages are 7 V and 6.5 V, respectively. (Popovic *et al.* 1998).

and both layers are missing, respectively. The turn-on voltage drops on introducing the ETL, but remains almost unchanged on inserting the HTL (Figure 4.4a) showing that contrary to the high hole injection rates across the anode/mixed-layer interface, which remain unchanged with or without a HTL, electron injection rates across the cathode/mixed-layer interface are much lower but can be increased by inserting the AlQ_3 ETL layer. On the other hand, the higher EL efficiency (from figure 4.4b) of structures (i) and (iii) relative to structures (ii) and (iv), respectively, shows the role of the HTL layer in reducing the leakage of electrons from the mixed layer to the anode. The EL efficiency increases more on inserting the ETL layer than on inserting the HTL (from the higher slopes of the L-J characteristics of (ii) relative to (iii)) indicating that the leakage of holes at the mixed-layer/cathode interface is more detrimental to the EL efficiency of the OLEDs than the leakage of electrons at the mixed-layer/anode interface. Therefore, the role of the HTL in improving the EL efficiency is mainly limited to blocking electrons, but the role of the ETL incorporates both blocking holes and enhancing electron injection. The higher EL efficiency on introducing the ETL may also be associated with the confinement of excitons away from the metal cathode where exciton quenching can take place effectively.

Another reason for the higher efficiency of the mixed-layer OLEDs can be due to the rise in the quantum efficiency of the AlQ_3 upon mixing with the NPB. The higher quantum efficiency is evident from the peak intensities of the normalised fluorescence spectra of AlQ_3 which progressively increase on reducing the AlQ_3/NPB ratio (Figure

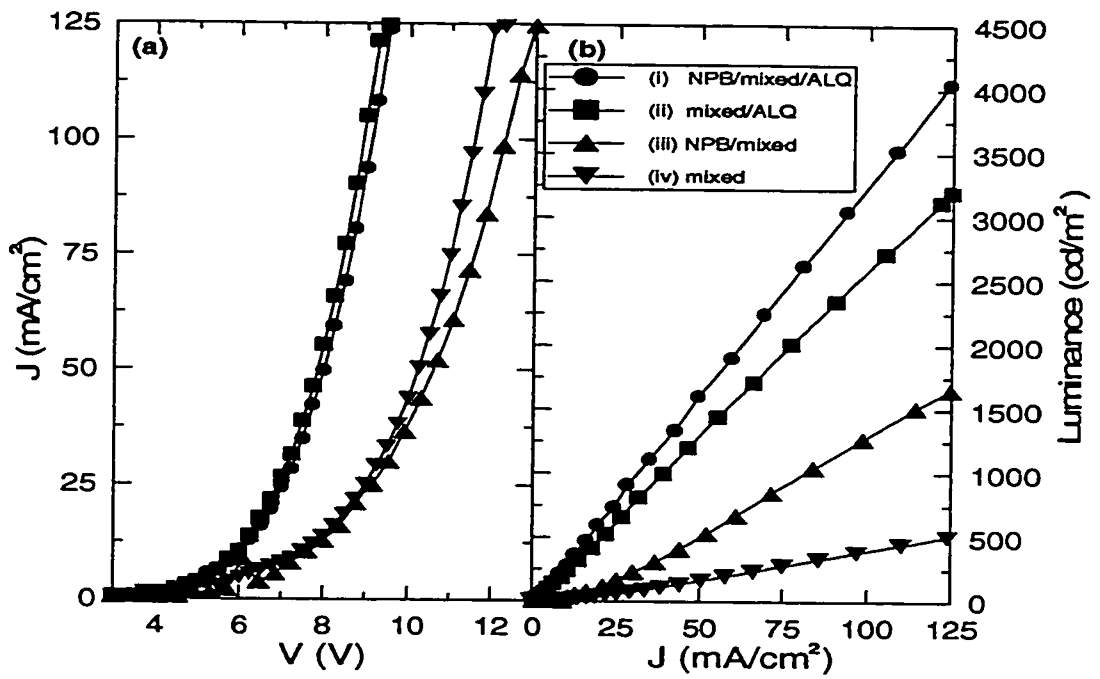

Figure 4.4: (a) J-V, and (b) L-J characteristics of OLEDs with the following structures: (i) anode /NPB (20nm) /mixed layer (80nm) /AlQ_3 (20nm) /cathode; (ii) anode / mixed layer (80nm) /AlQ_3(20nm)/ cathode; (iii) anode/ NPB(20nm)/ mixed layer (80nm)/ cathode; and (iv) anode/ mixed layer (100nm)/ cathode. Composition of the mixed layer is 50%NPB-50%AlQ_3 (by weight). (Popovic *et al.* 1998).

4.5). (The spectra are acquired using a 442 nm excitation (where NPB absorption is insignificant), and normalised to the various optical absorption levels of the corresponding mixed films at this wavelength). Because the drop in the PL intensity on increasing the AlQ_3 concentration is accompanied by a slight red shift of the spectra, the lower quantum efficiency of more concentrated AlQ_3 can be attributed to a concentration-quenching phenomenon due to excimer formation (Barltrop and Coyle 1978, Kalinowski *et al.* 1996-b).

4.1.4 Conclusions Pertaining to the Higher Stability of Mixed-Layer OLEDs:

The stability of the mixed-layer OLEDs is found to be largely independent of the mixing ratios of the NPB and the AlQ_3. The fact that the introduction of the mixed layer leads to a higher efficiency and an improved stability rules out the role of inter-layer diffusion in causing OLED degradation as was suggested before (Han *et al.* 1995-b, Do *et al.* 1996-b).

It can be argued that the higher stability of the mixed-layer OLEDs reported in this study is attributed to the fact in these devices, only a thin HTL (20 nm) of pure NPB is used (as opposed to 75 nm thick HTL of pure NPB in case of standard bilayer OLEDs). Being thinner, the HTL may, therefore, have a higher morphological stability. On the other hand, the presence of the hole transport material in the mixed layer may not necessarily have a detrimental effect on its stability, due to the entropy effect of mixing. Such argument comes in agreement with the widely accepted belief, discussed earlier

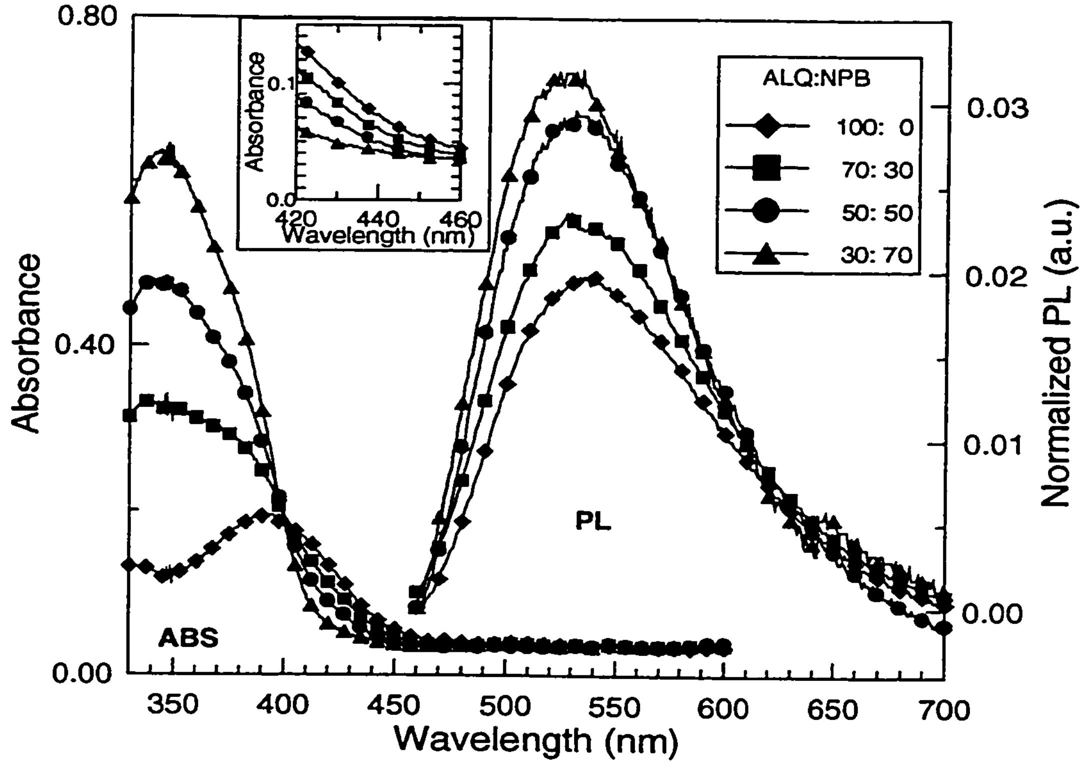

Figure 4.5: UV-Vis absorption and PL emission spectra (using 442 nm excitation) of 100 nm thick mixed films of various AlQ_3/NPB weight ratios deposited on quartz substrates. The PL spectra are normalised according to the corresponding absorption level of each film at 442 nm. The films absorbance is referenced to a base line of 0.04 corresponding to losses by the substrate. Absorption in the 420-460 nm range is magnified in the inset. (Popovic *et al.* 1998).

in section 1.2.2, that the poor morphological stability of the hole transport material is the major cause of degradation in OLEDs. To investigate the validity of such argument, lifetime tests are carried on a group of mixed-layer OLEDs with identical mixed layers and ETLs, but with HTLs of various thicknesses. From figure 4.6 it can be seen that increasing the thickness of the HTL leads to even more stable OLEDs. By using a 75 nm thick HTL, a lifetime of about 1400 hours is achieved, compared to about 550 hours for OLEDs with a 20 nm thick HTL. Since longer OLED lifetimes can be achieved by using thicker layers of pure hole transport materials, the morphological instability of such layers can not be the major cause of device degradation.

In fact, the higher stability of the mixed-layer OLEDs proves not only that the poor morphological stability of the hole transport material is not causing degradation, but also that the ITO/HTL interface is stable, even in the absence of an intermediate buffer layer. The instability of this interface has been another degradation suspect as previously discussed in section 1.2.2.

On the other hand, the higher OLED stability as a result of introducing a mixed layer between the HTL and the AlQ_3 layer shows that device degradation is caused by ageing processes at (or near) the HTL/ AlQ_3 interface in bilayer OLEDs. This conclusion is evident from the fact that the main difference between the bilayer devices and those with a mixed layer is the presence of such interface in the former but not in the later. To test the validity of this conclusion, devices consisting of thick pure NPB and AlQ_3 layers

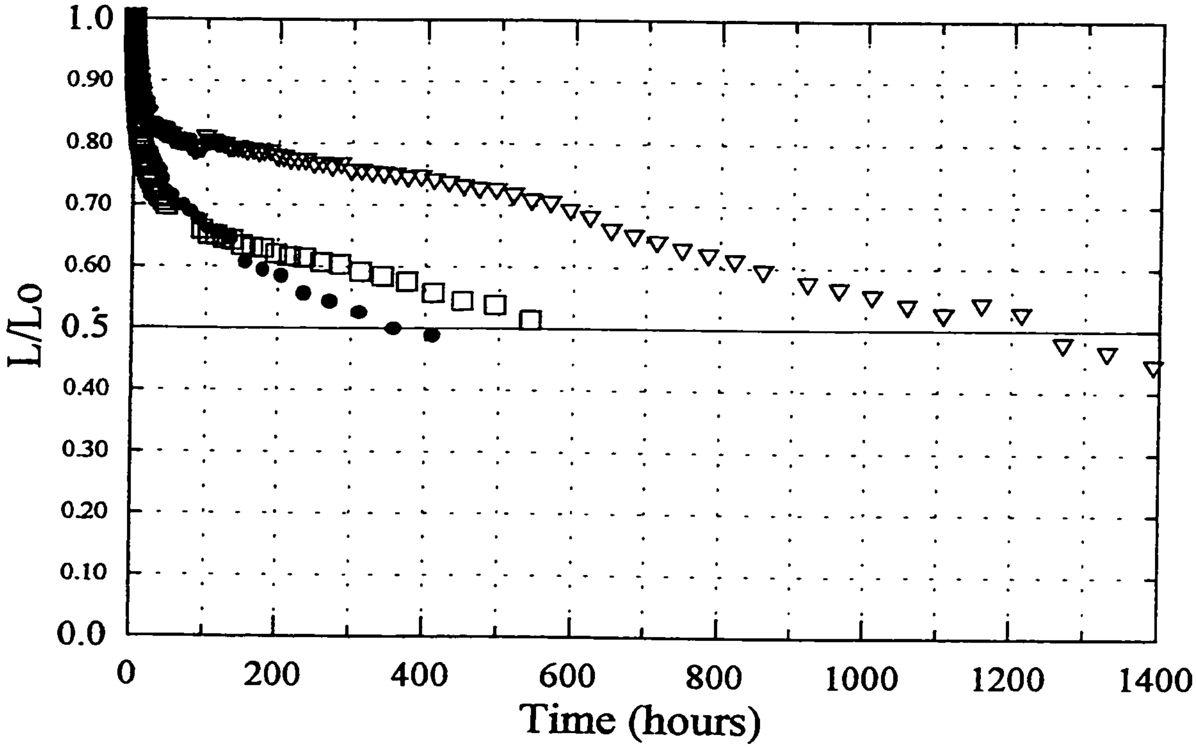

Figure 4.6: Luminance (L) / initial luminance (Lo) *vs.* time for mixed layer OLEDs consisting of anode /NPB (x) /mixed layer (80 nm)/AlQ_3 (20 nm) / cathode. x = 5 nm (●), 20 nm (□), and 75 nm (▽). Composition of the mixed layers is 50%NPB-50%AlQ_3 (by weight).

(75 nm and 80 nm thick, respectively) separated by a thin mixed layer (10 nm thick) are tested and compared to identical devices that do not have the mixed layer. A remarkable increase in stability is observed as a result of introducing the thin mixed layer at the NPB/AlQ_3 interface as shown in figure 4.7, thus proving the validity of the view that OLED degradation occurs mainly at or near the HTL/AlQ_3 interface.

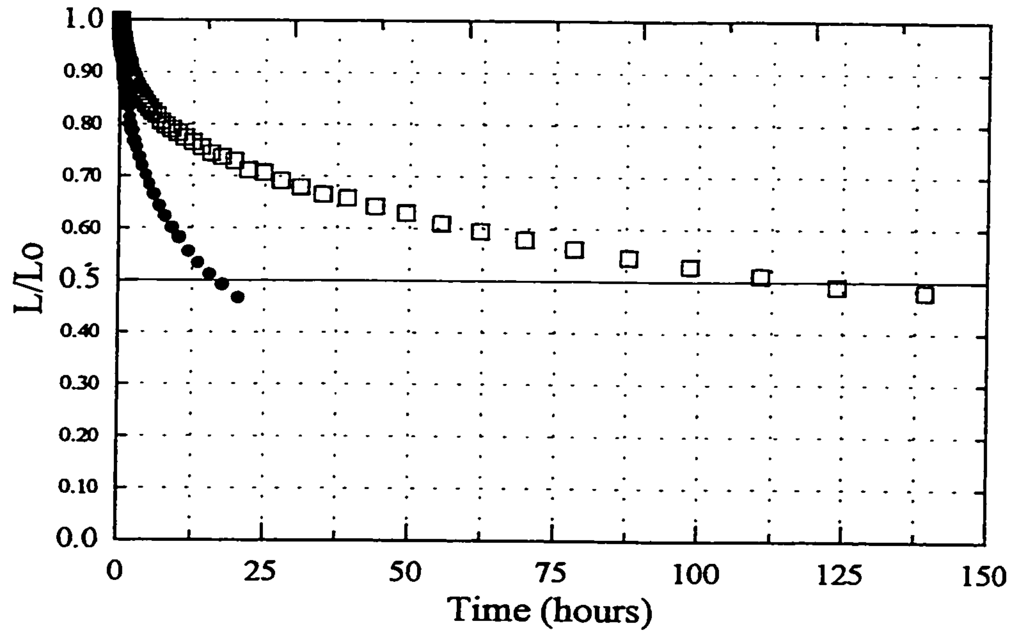

Figure 4.7: Luminance (L) / initial luminance (Lo) *vs.* time for OLEDs consisting of: anode /NPB (75 nm)/ AlQ_3 (80 nm) / cathode (•); and anode /NPB (75 nm)/ mixed layer (10 nm)/ AlQ_3 (80 nm) / cathode (□). Composition of the mixed layer is 50%NPB-50%AlQ_3 (by weight).

4.2 OLEDs with a Buffer Layer at the Hole-Injecting Contact or a Doped HTL†

So far, OLED aging is found to be essentially confined to the region near the HTL/AlQ_3 ETM interface. In order to understand the nature of the aging phenomena, it is important to understand the role of other OLED stabilizing approaches, namely; introducing a buffer layer at the ITO contact, and doping the HTL, in controlling such phenomena. A step towards understanding the effect of these stabilizing approaches on the performance of the OLEDs is to study their effect on the J-V-L characteristics of a device. Therefore, a comparative study is conducted on a group of OLEDs of various structures. These included devices with (1) a CuPc buffer layer (ca. 15 nm thick) layer at the ITO contact, (2) a rubrene-doped NPB layer (1% by mole), and (3) a standard bilayer structure. In all structures, the thickness of the NPB and AlQ_3 layers is 60 nm and 75 nm, respectively. To allow for a more accurate comparison between the different structures, all devices are fabricated in a single pump-down cycle and tested under the same conditions.

The *J-V* and *L-J* characteristics of the devices are shown in figure 4.8. Introducing a 15 nm layer of CuPc at the ITO contact is found to enhance the electroluminescence efficiency (4.2 cd/A for OLEDs with the CuPc layer compared to 3.1 cd/A for standard bilayer OLEDs). Because introducing the CuPc layer causes a shift in

---

† Reprinted with permission from [Aziz *et al.*, 1999, *Science* 283, 1900]. Copyright © [1999], The American Association for the Advancement of Science.

the *J-V* characteristics to higher voltages, it can be concluded that the CuPc impedes the injection of holes into the HTL. In principle, the shift in the *J-V* characteristics arises partially due to the thicker device in this case, however, this effect can be ignored because the increase in device thickness (~ 11 %), and hence the expected increase in the voltage required to drive the same current density, is small relative to the observed shift in the *J-V* characteristics (~ 65 % voltage increase). The higher electroluminescence efficiency is therefore attributed to the role of the CuPc in achieving more balanced electron and hole injection through impeding the injection of holes into the NPB (Vestweber and Rieb 1997). Doping the HTL with rubrene also leads to a shift in the *J-V* characteristics of the OLEDs to higher voltages, in agreement with the findings of Vestweber *et al.* This shift points to the role of the dopant molecules in forming hole traps, thus reducing their mobility in the HTL (Yang and Shen 1998). Similar to the case of OLEDs with a CuPc layer, doping the HTL also leads to a higher electroluminescence efficiency. However, unlike the case of CuPc, where the higher efficiency can be solely attributed to a more balanced electron and hole processes, the role of dopant molecules in enhancing the efficiency must be extended to include their role in the generation of light by acting as sensitizers or as electron-hole recombination sites (Hamada *et al.* 1995, Shi and Tang 1997, Murata *et al.* 1998). The fact that the shift in the *J-V* characteristics is much more pronounced in case of introducing the CuPc layer than in case of doping the HTL can be attributed to the different nature of the hole-impeding process in each case. The CuPc layer impedes the injection of holes into the HTL, but the dopant molecules reduce their mobility inside the HTL, the effect of which may not be as strongly reflected on the *J-V*

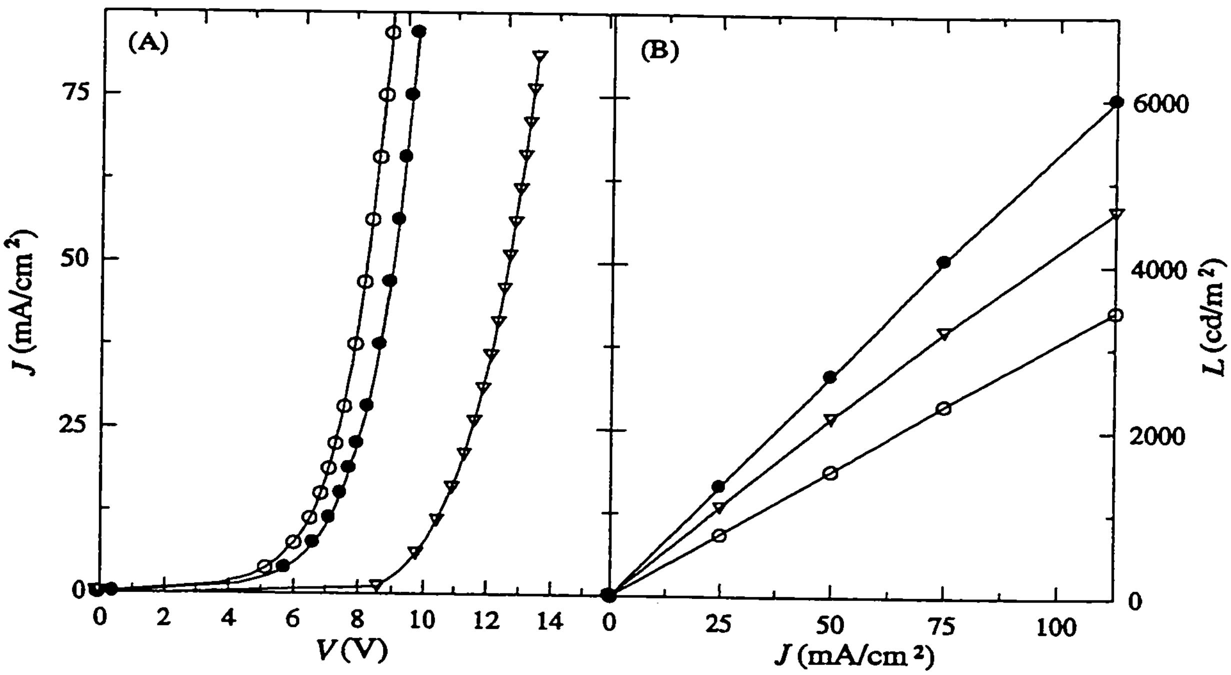

Figure 4.8: (a) *J-V*, and (b) *L-J* characteristics for anode/NPB/AlQ_3/cathode (O), anode/Rubrene – doped NPB/AlQ_3/cathode (●), and anode/CuPc (15nm)/NPB/AlQ_3/ cathode (V) OLEDs. In all devices, the thickness of the HTL and the AlQ_3 layer is 60 nm and 75nm, respectively. (Aziz *et al.* 1999-a).

characteristics due to the superior hole mobility characteristics of NPB (Malliaras and Scott 1998). It should be pointed out that the shift of the *J-V* characteristics to higher voltages in case of introducing the CuPc layer or doping the HTL does not contradict the fact that these stabilizing agents, due to the efficiency enhancement, may seem to lower the luminance turn-on voltage of the OLEDs. According to these results, it can be concluded that a common feature of the role of these two stabilizing agents is to impede the transport of the holes and thus to slow down their transport to the HTL/AlQ_3 interface where they get injected into the AlQ_3 layer. From these results, it is possible to postulate that the injection of holes into the AlQ_3 layer is the main factor responsible for OLEDs degradation. In fact, this postulate is consistent with an earlier study which shows, from cyclic voltammetry on AlQ_3 in solutions, that the oxidation of AlQ_3 is irreversible (Papadimitrakopoulos *et al.* 1996, Anderson *et al.* 1998).

CHAPTER 5

The Mechanism of Intrinsic Degradation in AlQ_3-Based OLEDs

From the findings presented in the previous chapter, the injection of holes into the AlQ_3 layer appears to be the main cause of device degradation. In the first section of this chapter, the experimental results verifying the validity of this postulate are presented. In view of these findings, the role of the various approaches in improving OLEDs stability is explained in the second section. In the following section, the proposed degradation mechanism is used to explain other observations pertaining to OLEDs stability; phenomena that were reported before but could not be explained in terms of the earlier OLED degradation theories available at that time. In the last section of this chapter, novel approaches to improve OLED stability, based on the new understanding of the degradation mechanism, are demonstrated.

The material contained in this chapter has been published or submitted for publication before. The material in the first three sections has been modified from the original manuscript entitled: "*Degradation Mechanism of Small Molecule-Based Organic Light Emitting Devices*" by: Hany Aziz, Zoran D. Popovic, Nan-Xing Hu, Ah-Mee Hor, and Gu Xu, published in 1999, in *Science*, Volume **283**, pp 1900-1902, where necessary modifications have been made to make it consistent with the general theme of this thesis. The material in the last section has been modified from the original manuscript entitled: "*Long-term Degradation Mechanism of Organic Light Emitting Devices Based on Small Molecules*" by: Hany Aziz , Zoran D. Popovic, Nan-Xing Hu, Ah-Mee Hor, and Gu Xu, submitted for publication in April 1999, in *Proceedings of the MRS Spring Meeting, Organic Light-Emitting Materials and Devices II,* San Francisco, CA, April 1999, where necessary modifications have been made to make it consistent with the general theme of this thesis. All the work presented in this chapter; device architecture, sample preparation, set-ups, measurements, analysis of results and the writing were entirely performed and contributed by the author under supervision of Dr. Zoran Popovic. The author acknowledges the contribution of Nan-Xing Hu in the synthesis of the organic raw materials.

5.1 Degradation of ALQ_3 Layers Under Hole Currents[†]

To test the effect of holes on the AlQ_3 layers of the OLEDs, special devices in which predominantly holes are transported through a thin AlQ_3 layer are constructed (Figure 5.1). In these devices, a 5-nm-thick AlQ_3 layer is placed between two layers of NPB. The lower 20-nm-thick NPB layer facilitates the injection of holes from the ITO anode into the AlQ_3 layer, whereas the upper 40-nm-thick layer both transports the holes from the AlQ_3 layer to the cathode and blocks electrons from reaching the AlQ_3 layer. The blocking of electron transport by NPB is incomplete, however. Some electrons still reach the middle AlQ_3 layer and cause weak EL. Because the NPB/cathode contact is unstable and usually creates shorted devices, a thin buffer layer of AlQ_3 (10 nm thick) is used between the upper NPB layer and the cathode.

In situ PL measurements (performed with 442 nm Hg-line excitation, where NPB absorption is negligible) are employed to monitor changes in the PL quantum efficiency of the 5-nm-thick AlQ_3 layer. A gradual decrease in the peak height of the PL spectra of AlQ_3 (Figure 5.2, spectra a to c) reveals a continuous decrease in the PL efficiency of the AlQ_3 after prolonged current flow. Other OLEDs consisting of only a 60-nm-thick NPB layer and a 10-nm-thick AlQ_3 top layer are also tested under the same conditions to check if PL from the top AlQ_3 contributed to the signal (Fig. 5.2, spectrum d). The 10-nm AlQ_3

[†] Reprinted with permission from [Aziz *et al.*, 1999, *Science* 283, 1900].

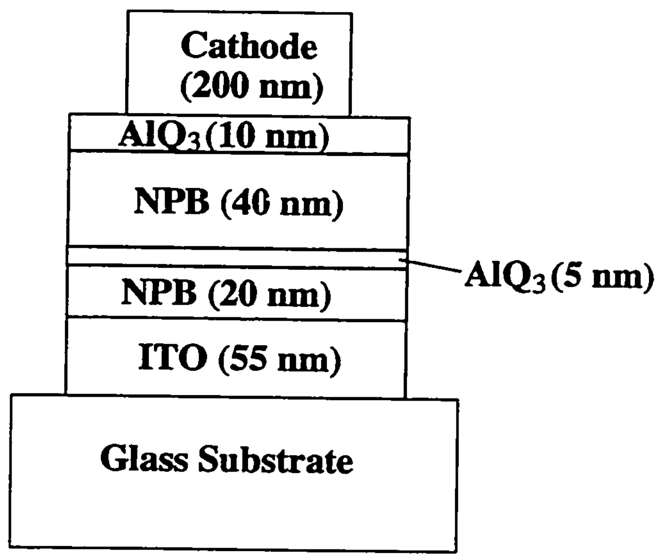

Figure 5.1: Structure of OLEDs used for photoluminescence measurements. (Aziz *et al.* 1999-a).

top layer, in contact with the metal cathode, contributes negligibly, probably because of exciton quenching by the metal due to the relatively large exciton diffusion length of AlQ_3 (Tang *et al.* 1989). Thus spectra a to c in figure 5.2 correspond to PL of the 5-nm AlQ_3 layer. The decrease in the PL quantum efficiency of this layer points to degradation as a result of current flow. As this layer transports predominantly holes, the observed fluorescence decrease indicates that cationic AlQ_3 species are most likely leading to formation of fluorescence quenchers. In principle another mechanism of fluorescence decrease is also possible, the formation of high concentration of non-emitting degradation products, which are not fluorescence quenchers. This mechanism would require that approximately half of AlQ_3 molecules decompose in order to produce the decrease in the PL quantum efficiency shown in figure 5.2. This possibility has been investigated by using infrared spectroscopy to detect any changes in the absorption spectra of AlQ_3 after degradation. The results show no detectable changes in the spectra, thus suggesting that the number of degraded AlQ_3 molecules is not substantial but limited to few that acted as fluorescence quenchers. This notion can be further investigated by using time-resolved photoluminescence measurements for detecting changes in the lifetime of the excited states and hence in obtaining a better understanding of the nature of the quenching species.

Identical devices in which the Mg:Ag cathodes are replaced by pure Ag cathodes are fabricated and tested under the same current driving conditions. Because of the higher work function of Ag compared to Mg:Ag (4.2 eV and 3.7 eV, respectively), the

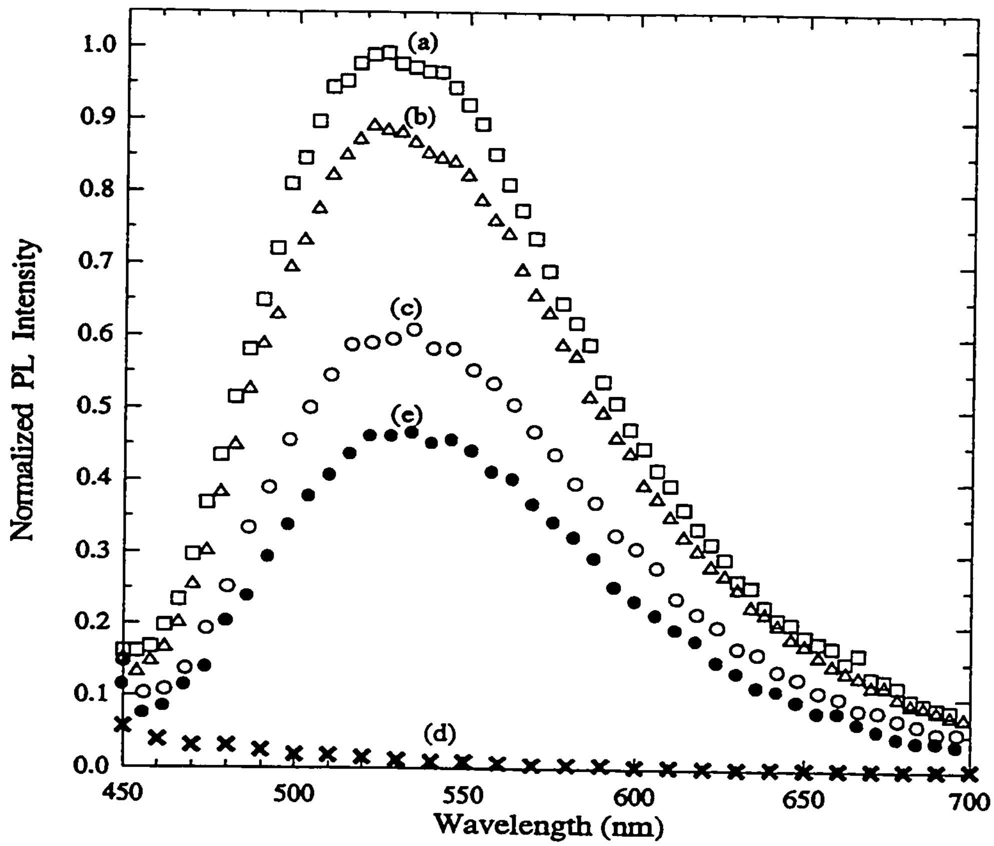

Figure 5.2: Normalized photoluminescence spectra of AlQ_3 in a device from figure 5.1 with Mg:Ag cathode, driven at 50 mA/cm^2, obtained (a) before stressing, (b) after stressing for 10 hours, and (c) after stressing for 50 hours. (d) Spectrum obtained from an OLED without the middle AlQ_3 layer. (e) PL spectrum of a device from figure 5.1 with an Ag cathode, obtained after stressing for 50 hours, driven at the same current density of 50 mA/cm^2. Spectra b to e are normalized to the peak photoluminescence before stressing the devices. (Aziz *et al.* 1999-a).

injection of electrons from the cathode into the organic layers is reduced, which leads to even more unbalanced current with a higher hole/electron ratio. The PL intensity of the AlQ_3 decreased to 45% of the initial level, in case of the devices with the Ag cathode (figure 5.2, spectrum e). In comparison, when a Mg:Ag cathode was used, PL decreased less, to 60% of the initial value over the same period of time (Figure 5.2, spectrum c). This result clearly shows that higher hole/electron ratios lead to a faster degradation of the AlQ_3, thus supporting the conclusion that cationic AlQ_3 species are unstable.

Because AlQ_3 is an excellent electron transport material (Bin *et al.* 1997), the transport of electrons through it is not expected to cause degradation. To prove the validity of this assumption, other similar devices, in which 5-nm-thick AlQ_3 layers are placed between two layers of an electron transport material, thus allowing only electrons to be transported through the AlQ_3, are tested. The results do not show any decrease in the PL quantum efficiency under similar current driving conditions, proving that the transport of electrons does not have a similar effect.

5.2 The Role of the Various Approaches for Improving OLEDs Stability†

The role of doping the HTL or introducing a thin buffer layer of CuPc at the hole-injecting contact in improving OLEDs stability can be explained in terms of slowing

† Reprinted with permission from [Aziz *et al.*, 1999, *Science* 283, 1900]. Copyright © [1999], The American Association for the Advancement of Science.

down the hole transport to the HTL/AlQ_3 interface. Under these conditions, the density of electrons in the AlQ_3 layer adjacent to the HTL/AlQ_3 interface is increased, leading to rapid recombination and therefore a shorter lifetime of the unstable cationic AlQ_3 species. It is also possible that because of the high electron density at the HTL/AlQ_3 interface, the production of cationic AlQ_3 species is greatly reduced, as holes can be injected directly from NPB into anionic AlQ_3 species to produce excited states (Anderson *et al.* 1998). This last effect is probably the dominant mechanism for improved stability of OLEDs with a mixed layer. In addition to improved carrier balance, holes in the mixed layer will preferentially reside on NPB sites because of the lower ionization potential of the NPB relative to that of AlQ_3 [5.1 eV and 5.7 eV, respectively, (Van Slyke *et al.* 1996, Vestweber and Rieb 1997)], whereas electrons will reside on AlQ_3 sites. As in the mixed layer NPB and AlQ_3 molecules are in close proximity, the direct recombination of holes and AlQ_3 anions to produce excited states of AlQ_3 directly will be a dominant recombination process.

5.3 Explaining Other Earlier Phenomena Pertaining to the Same Mechanism†

5.3.1 The Correlation Between the Ionization Potential of the HTL and OLED Stability:

Adachi *et al.* observed the presence of a correlation between a lower ionization potential of the HTL and a higher OLED stability (Adachi *et al.* 1995). Although such

† Reprinted with permission from [Aziz *et al.*, 1999, *Science* **283**, 1900]. Copyright © [1999], The American Association for the Advancement of Science.

observation could not be explained in terms of the (then widely believed) morphological instability of the HTL, it can be easily explained in terms of the proposed degradation mechanism. In this case, a lower ionization potential of the HTL leads to a more difficult injection of holes into the AlQ_3 as a result of a higher hole injection barrier at the HTL/AlQ_3 interface. The reduced injection of holes into the AlQ_3 layer leads to a higher density of electrons in the AlQ_3 layer adjacent to the HTL/AlQ_3 interface, which, in turn, leads to a faster recombination, and therefore a shorter lifetime of cationic AlQ_3 species. As a result, AlQ_3 degradation is reduced, leading to longer OLED lifetimes.

5.3.2 The Correlation Between the Work Function of the Cathode and OLED Stability:

Matsumura and Jinde observed the presence of a correlation between a lower work function cathode material and a higher OLED stability (Matsumura and Jinde 1997). According to the proposed degradation mechanism, the increase in device stability on using metals with lower work function for the cathodes can be attributed to an easier injection of electrons from the cathode into the AlQ_3 layer. This leads to a higher density of electrons in the AlQ_3 layer adjacent to the HTL/AlQ_3 interface; hence a faster recombination and a higher device stability.

5.4 Demonstrating the Degradation Mechanism Using Dual-Layer HTL Structures†

OLEDs with HTL consisting of two layers (referred to as dual-layer HTL) of

† Submitted for publication in *Proceedings of MRS* (April, 1999). No copyright transfer has been released.

different hole transport materials with dissimilar ionization potentials. Depending on the order of the two layers, the transport of holes to the AlQ_3 layer can be either facilitated or impeded, thus leading to significantly different OLED lifetimes.

To demonstrate this effect, OLEDs with a dual HTL consisting of separate layers of pure NPB and pure TPD are constructed in two different arrangements to obtain ITO/NPB/TPD/AlQ_3/Mg:Ag (referred to as structure A) and ITO/TPD/NPB/AlQ_3/Mg:Ag (referred to as structure B) OLED structures (Figure 5.3). Because of the higher ionization potential of TPD relative to that of NPB [5.6 and 5.1 eV, respectively, (Shirota *et al.* 1994, Van Slyke *et al.* 1996)], structure A is expected to enhance the injection of holes into the AlQ_3 layer by means of hole cascading. On the other hand, due to the relatively high hole injection barriers at the ITO/TPD and at the NPB/AlQ3 interfaces in structure B, injection of holes into the AlQ_3 layer would be reduced. Therefore, according to the proposed degradation mechanism, OLEDs of structure B should be more stable than OLEDs of structure A.

Lifetime measurements reveal that this indeed is the case, where OLEDs of structure B demonstrate lifetimes that are approximately five times longer than OLEDs of structure A, both fabricated on the same substrates during the same pump-down cycle (Figure 5.4). Therefore, using a dual-layer HTL is not only another proof of the validity of the proposed degradation mechanism, but can also be employed as a new approach to improve OLED stability.

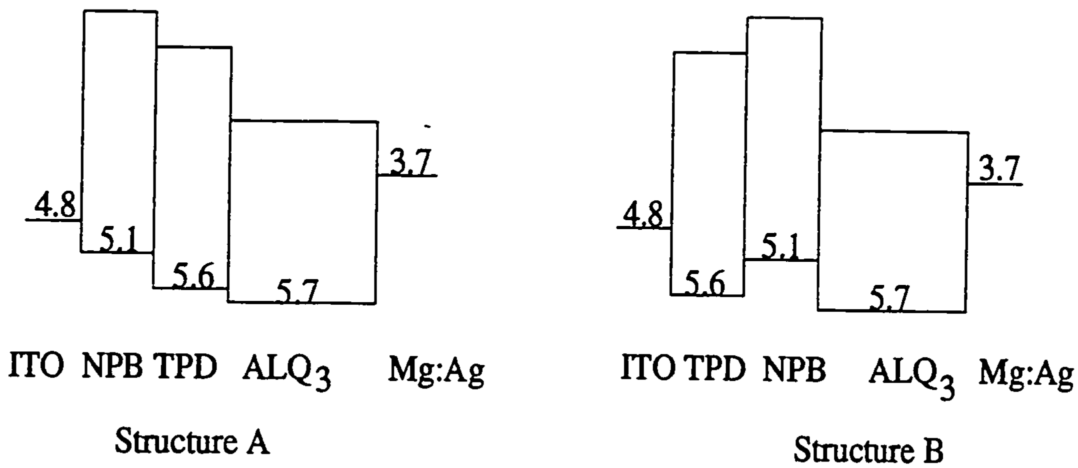

Figure 5.3: Energy levels of dual-layer HTL OLEDs. The numbers refer to the ionization potential of the organic layers and the Fermi levels of the electrodes (in eV) (Aziz *et al.* 1999-b).

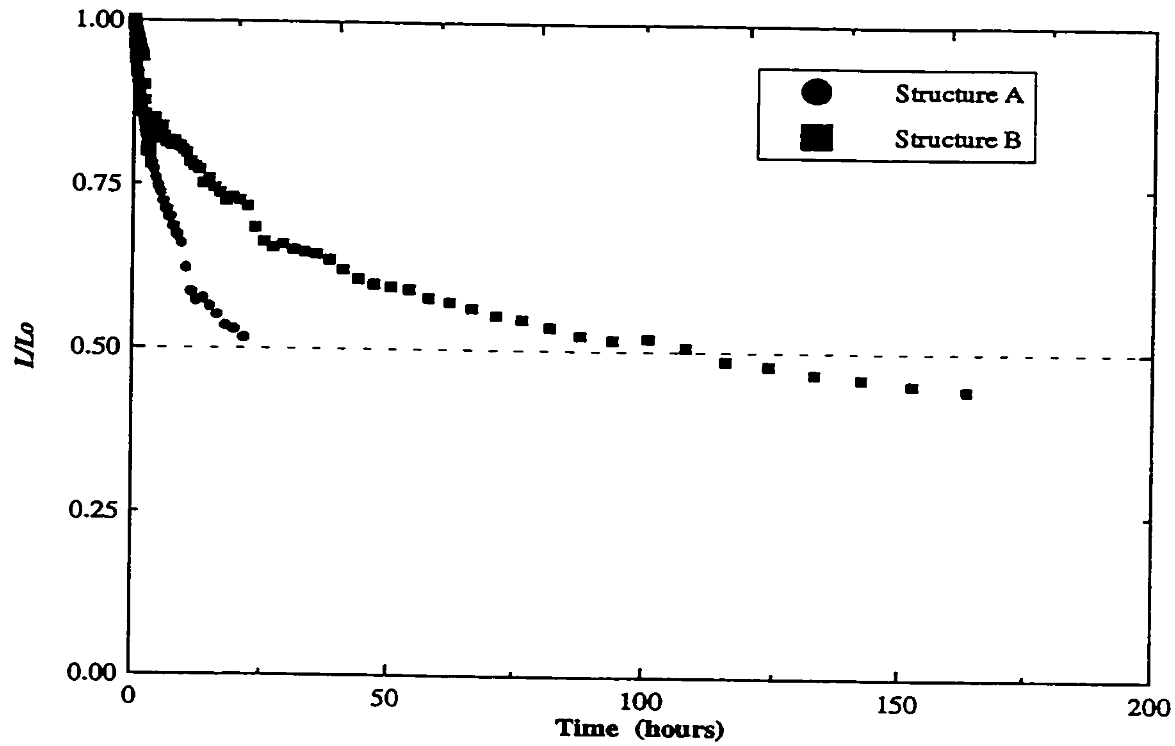

Figure 5.4: Luminance (*L*)/initial luminance (*Lo*) *versus* time for dual-layer HTL OLEDs of structures as shown in figure 5.3, both operated using constant dc current of 25 mA/cm^2. In both structures, the thickness of the NPB, TPD, and AlQ_3 layers is 30, 30, and 75 nm, respectively. Lo of both OLEDs is about 710 cd/m^2 (Aziz *et al.* 1999-b).

CHAPTER 6

Discussion of a Theoretical Framework to Model Degradation in OLEDs

An important aspect of studying the degradation mechanism in OLEDs is to be able to lay the foundation for developing a theoretical framework that models device aging. Such model would be useful in comparing experimental data to theory, and hence in refining our understanding of the degradation processes. It would also be useful in setting the design rules for future OLED manufacturing processes on the basis of analytical rather than empirical correlations. Developing such a model for device degradation, however, is not possible without first having a theoretical foundation that accurately describes charge injection and transport across the different layers and interfaces of the OLED, which is, unfortunately, still unavailable. Although few studies focused on developing such theoretical foundation (Kalinowski *et al.* 1996, Scott *et al.* 1997, Malliaras and Scott 1998, Yang and Shen 1998, Kawabe *et al.* 1998), they were essentially limited to single layer devices, and, therefore, never described charge injection phenomena across the HTL/AlQ_3 interface where degradation mainly occurs.[†]

[†] During the final stages of preparing this thesis, it came to the author's knowledge that the results of a preliminary theoretical study addressing the organic/organic heterojunction has recently been submitted for publication (Yang and Shen 1999), and that a more comprehensive study, including formalisms, is currently underway and may be published by the end of 1999 (Shen 1999).

Developing such a model for degradation is outside of the scope of this work. Instead, this chapter only provides an outline of the important features that must be addressed in any theoretical treatment aiming at modeling OLED degradation. In the first section of this chapter, a framework for correlating the degradation rate of OLED, which appears as decay in device luminance with time, to microscopic phenomena is discussed. In the second section, a theoretical background for determining electron and hole concentration profiles across the OLED is provided.

6.1 Phenomena Governing the Kinetics of OLED Degradation

In the preceding chapters, it has been established that degradation in the OLEDs is caused by the formation of the unstable AlQ_3^+ species produced by the injection of holes into the AlQ_3 layer in the vicinity of the HTL/AlQ_3. Although the exact mechanism of this process is not known at present, it has been shown that the degradation products (denoted by Q) act as fluorescence quenchers of the excited AlQ_3 molecules which reside in their vicinity. To model their quenching effect, the individual Q species can be visualized as having an effective volume, with a characteristic radius (effective radius) r_Q. The luminescence of the AlQ_3 molecules within this volume is quenched, and therefore do not contribute to device luminance. The exciton quenching can be assumed to occur through an energy transfer process from these AlQ_3 molecules to the Q species via a Förster or a Dexter process as it is usually the case in organic systems (Pope and Swenberg 1982). If a Förster process is the dominant mechanism, r_Q will be in the order of 10 nm. On the other hand, if energy transfer from the excited molecules to the Q species occurs mainly via a Dexter process, r_Q will be in the order of 1 nm (Bulovic 1998). The diffusion of excitons towards the Q species can also be involved in the quenching process. In this case, r_Q will be in the order of the exciton diffusion length, equal to $(D\tau)^{1/2}$, where D is the diffusion coefficient and τ is the exciton lifetime. Both D and τ can be determined experimentally. Exciton diffusion can also contribute to the quenching effect by causing the migration of excitons to the vicinity of the Q species where Förster or Dexter processes become more effective.

In general, the transition of an AlQ_3 molecule in an excited electronic state to the ground state can occur via radiative or non-radiative processes. The non-radiative transitions include intramolecular processes (e.g. internal conversion), intermolecular processes between different AlQ_3 molecules (e.g. triplet-triplet annihilation), and intermolecular processes between AlQ_3 molecules and Q species. Since these processes compete together on the population of the excited AlQ_3 molecules, their relative rates (reflected in their rate constant) determines the dominance of one or more process in carrying the transition. These processes can be represented as:

$$[AlQ_3^*] \xrightarrow{k_f} [AlQ_3] + h\nu \quad \text{(radiative)} \qquad (6.1)$$

$$[AlQ_3^*] \xrightarrow{k_{nr}} [AlQ_3] + \text{heat} \quad \text{(non-radiative, intra- and inter-molecular processes involving } AlQ_3 \text{ molecules only)} \qquad (6.2)$$

$$[AlQ_3^*] \xrightarrow{k_Q\,[Q]} [AlQ_3] + \text{heat} \quad \text{(non-radiative, intermolecular processes involving } AlQ_3 \text{ and Q species)} \qquad (6.3)$$

where k_f, k_{nr} and k_Q are the rate constants of the radiative (fluorescence process), of nonradiative intramolecular and intermolecular processes involving AlQ_3 molecules only, and of nonradiative intermolecular processes involving both AlQ_3 and Q species (quenching process), and [Q] is the concentration of the Q species. The first two processes obey first order kinetics, and, therefore, their rates are given by $k_f.[AlQ_3^*]$ and $k_{nr}.[AlQ_3^*]$, respectively, where $[AlQ_3^*]$ is the concentration of excited AlQ_3 molecules. The third process depends on both k_Q and the concentration of the Q species. Its rate is linear in Q, in the first approximation, and is given by $k_Q.[Q].[AlQ_3^*]$ (Barltrop and Coyle 1978). The yield of the radiative process (η_f) is equal to:

$$\eta_f \quad = \quad k_f \,/\, (\, k_f + k_{nr} + k_Q.[Q]\,) \qquad (6.4)$$

Clearly, a high η_f is required for efficient electroluminescence in an OLED. On the other hand, an increase in the concentration of the Q species leads to an increase in the rate of the quenching process, and results in a lower quantum efficiency. Therefore, quantifying the rate of luminance degradation in an OLED requires calculating the rate of formation of the Q species.

The chemical reactions involved in the formation of the Q species as a result of the degradation of the cationic AlQ_3 species, referred to later as the AlQ_3 degradation process, can be collectively expressed as:

$$AlQ_3^+ \rightarrow Q \qquad (AlQ_3^+ \text{ degradation process}) \qquad (6.5)$$

This process can be a simple concerted formation of products from reagents, or it may occur through one or more intermediates which may also be able to revert to the starting AlQ_3 species. Because the reaction mechanism is unknown, and hence the rates of the different steps involved, a collective reaction rate R_Q will be used. It should be pointed that R_Q is the collective rate of the chemical reactions producing the Q species from AlQ_3^+, and should not be confused with the quantity { k_Q.[Q].[AlQ_3*] } which represents the rate of the photophysical processes leading to quenching the excited molecules due to the presence of Q.

In the AlQ_3 layer of an OLED, the rate of production of the Q species depends not only on the rate of the AlQ_3 degradation process but also on the recombination process of the hole *(h)* on the AlQ_3^+ and an electron *(e)* from a neighboring AlQ_3^- species to produce excited AlQ_3* molecule:

$$AlQ_3^+ + AlQ_3^- \rightarrow AlQ_3^* + AlQ_3 \qquad (\text{Recombination Process}) \qquad (6.6)$$

The rate of this process is denoted by R_{eh}. Because this process competes with the AlQ_3 degradation process on the available AlQ_3^+ population, the rate of formation of the Q species is reduced. The reduced rate, R_Q', is related to R_Q through a correction factor f_Q such that:

$$R_Q' = f_Q \,.\, R_Q \qquad \text{where} \qquad f_Q = R_Q / (R_Q + R_{eh}) \tag{6.7}$$

The relative magnitudes of R_Q and R_{eh} are critical to OLED stability. For $R_Q >> R_{eh}$, R_Q' is almost equal to R_Q and the degradation process is essentially not slowed down by the recombination process. Obviously, in a stable OLED, R_{eh} must be many orders of magnitude greater than R_Q. The rate of OLED degradation will therefore be governed by R_Q' rather than R_Q.

The magnitude of R_{eh} depends on the nature of the recombination process. In organic materials, as in the AlQ_3 layer of an OLED, the oppositely charged carriers are statistically independent of each other, and the carrier recombination process follows bimolecular kinetics. Therefore, in the first approximation, the recombination processes can be explained by the simple Langevin theory (Pope and Swenberg 1982). According to this theory, the electrons and holes diffuse towards each other by attractive Coulombic interaction because the carrier mean free path is smaller than the radius of capture of one carrier by the other. Since the carriers thermalize quickly, the recombination may be viewed as the drift of two carriers together under the action of the Coulombic field. In effect, the holes can be viewed as stationary and only the electrons move with an effective mobility μ_T equal to the sum of the electron and hole mobilities (i.e. $\mu_T = \mu_e + \mu_h$ where e and h represent electron and hole, respectively). In this model, the electron hole recombination rate R_{eh} is given by

$$R_{eh} = \Upsilon_{eh}\,[AlQ_3^{+}]\,[AlQ_3^{-}] = \Upsilon_{eh}\,p\,n \tag{6.8}$$

where Υ_{eh} is the bimolecular rate constant for free hole electron recombination, and p and n represent the concentration of free electrons and holes, respectively (equal to the concentrations of cationic and anionic AlQ_3, respectively). Υ_{eh} is given by:

$$\Upsilon_{eh} = \mu_T\, e\,(\varepsilon\,\varepsilon_o)^{-1} \tag{6.9}$$

where e is the electron charge, ε is the dielectric constant of AlQ_3, and ε_o is the permittivity of vacuum.

It should be pointed that, in the Langevin theory, the electrons and holes are driven towards each other by attractive coulombic interactions in the absence of other electric fields. In an OLED, however, the recombination rate will be lower than that given by equations (6.8) and (6.9) due to the probability of escape of a charge carrier from its counter carrier under the influence of the applied electric field. A more accurate description of the recombination process, therefore, requires a field-dependent recombination rate according to the Onsager formalism (Borsenberger and Weiss 1998). In addition, in amorphous organic materials, the mobility of charge carriers depends on the electric field because the average barrier height for energetic jumps decreases at higher fields. The dependence of the mobility on the electric field is typically expressed as

$$\mu = \mu_o \exp\left(\alpha F^{1/2}\right) \tag{6.10}$$

where F is the electric field, and the coefficients μ_o (termed the zero field mobility) and α are determined experimentally. A more realistic description of the recombination process in an OLED, therefore, also requires replacing the constant mobility coefficient in equation (6.8) by a field dependent mobility according to equation (6.10). However, due to mathematical complexities, no analytical solutions have, so far, been developed for a Langevin recombination model with a field-dependent mobility.

From the preceding discussion, calculating the rate of formation of the Q species (in order to determine OLED degradation rate) requires determining R_Q' which, according to equation (6.7), depends on R_Q and R_{eh}. R_Q depends on the concentration of holes, whereas R_{eh} is governed by the concentrations of both holes and electrons. In the AlQ_3

layer of an OLED, these concentrations vary across the layer thickness, and hence the concentration profiles of the Q species will also be position dependent.

6.2 Charge Carrier Distribution in an OLED

The distribution of charge carriers across the organic layers depends on the charge injection, transport and recombination phenomena. In general, conduction in an OLED can be limited by either the injection processes at the interfaces (i.e. injection-limited) or by transport processes in the bulk (i.e. bulk-limited) (Kalinowski *et al.*, 1996). A conclusive answer to whether an injection-limited or a bulk-limited case is the more dominant scenario in OLEDs is still not available (Burrows and Forrest 1994, Mori *et al.* 1995, Kalinowski *et al.* 1996, Ioannidis *et al.* 1998, Campbell and Smith 1999, Yang and Shen 1998). However, due to the low carrier mobility in the organic layers ($\mu_e \sim 10^{-5}$ $cm^2/V.s$ for AlQ_3), which results in a carrier distribution that decays rapidly into the bulk away from the injecting electrode, a space-charge is formed. As a result, conduction can be described using a model of a space charge limited current (SCLC) (Kao and Hwang 1981, Kalinowski *et al.* 1996, Scott *et al.* 1997, Shen and Yang 1998).

6.2.1 Governing Equations:

Double-carrier conduction in an organic layer, according to the SCLC model, is governed by the following equations:

(i) The current flow equations:

$$J_e = e\,\mu_e\,n\,F \qquad (6.11)$$

$$J_h = e\,\mu_h\,p\,F \qquad (6.12)$$

$$J = J_e + J_h \qquad (6.13)$$

(ii) Poisson's equation:

$$\frac{dF}{dz} = -\frac{d^2\Psi}{dz^2} = -\frac{e\,[p + p_t - n - n_t]}{\varepsilon} = \frac{\varrho}{\varepsilon} \qquad (6.14)$$

(iii) The current continuity equations:

$$\frac{1}{e}\frac{dJ_e}{dz} = \frac{-1}{e}\frac{dJ_h}{dz} = R_{eh} \qquad (6.15)$$

In these equations, J_e is the electron current density, J_h is the hole current density, e is the electron charge, F is the electric field, Ψ is the electrostatic potential (defined to be $-E_i/e$ where E_i is the intrinsic Fermi level) , and ϱ is the total charge density, which is the sum of p, p_t, n, and n_t , the concentration of free holes, trapped holes, free electrons and trapped electrons, respectively. R_{eh} is the recombination rate previously defined in equation (6.8). In these equations, z represents the distance across the thickness of the layer from some arbitrary reference plane. Although the total current density J is constant throughout the organic layer, the quantities J_e , J_h , F , p, p_t, n, and n_t all vary across the thickness and thus are functions of z. In the current continuity equation, the decrease in the hole current has been attributed solely to the recombination of AlQ_3^+ with AlQ_3^-, whereas the contribution of the degradation of AlQ_3^+ into Q has been ignored. This assumption can be justified in view of the fact that, in a real OLED, the rate of the recombination process (R_{eh}) is many orders of magnitude greater than the rate of the degradation process (R_Q).

Determining the rate of the degradation in an OLED, therefore, requires calculating the spatial profiles of *F*, *n* and *p* by solving the above equations. These equations do not lend themselves to analytical solutions, except for simple hypothetical cases, such as, a case of a trap-free SCLC conduction in a single layer OLED (Scott *et al.* 1997). As a result, mathematical expressions for determining *F*, *n* and *p* profiles in a real OLED are not yet available. Numerical solutions are therefore attempted (Kawabe *et al.* 1998, Shen and Yang 1998, Malliaras and Scott 1998, Yang and Shen, 1998, *ibid.* 1999-a). On the other hand, a more realistic model of conduction in OLEDs also requires using a field-dependent mobility, and hence further mathematical complexities. Developing a mathematical model for OLED degradation is, therefore, not within the scope of this work. Instead, important parameters that should be considered in solving these equations, either numerically or analytically, will be addressed for three important OLED cases. These cases are: (1) A standard bilayer OLED, (2) A device with a buffer layer or a dual layer HTL, and (3) A device with a doped HTL.

6.2.2 The Case of a Standard Bilayer OLED:

Modeling conduction in a bilayer device can be approximated by treating a bilayer device as two single layer devices that can be modeled independently except for having a common set of boundary conditions to account for the HTL/AlQ_3 interface. In this case, the AlQ_3 layer can be modeled by a double-carrier current injection SCLC and is therefore governed by equations (equations 6.11 through 6.15). On the other hand, because the electron mobility in the HTL is much lower than the hole mobility, electron currents in the HTL, which are essentially unimportant in device degradation, can be ignored, and thus the HTL can be modeled by a single-carrier current injection SCLC. Therefore, the governing equations for the HTL reduce to:

(i) the current flow equations:
$$J_h = e\,\mu_h\,p\,F = J \qquad (6.15)$$

(ii) Poisson's equation:
$$\frac{dF}{dz} = \frac{e\,[p + p_t]}{\varepsilon} = \frac{\varrho}{\varepsilon} \qquad (6.16)$$

Solving the governing equations for each of the two layers requires knowing the corresponding boundary conditions. Boundary conditions at the metal contacts can be obtained from the expressions for the appropriate injection mechanism. In OLEDs, quantum mechanical tunneling is believed to be the dominant injection mechanism (Kalinowski *et al.* 1996, Campbell *et al.* 1998), and therefore, the electric field, both in the HTL at the ITO contact and in the AlQ_3 layer at the cathode contact, can in the first approximation be determined by using the Fowler-Nordheim equation for each of the two contacts (Kawabe *et al.* 1998):

$$J = \frac{2.2\, e^2 F_o^2}{8\, \pi h\, \Phi} \exp\left[- \frac{8\, \pi\, (2\, e\, m^*)^{1/2}\ \Phi^{3/2}}{3\, h\, F_o} \right] \tag{6.17}$$

where F_o represents the electric field F in the HTL at the ITO contact or in the AlQ_3 layer at the cathode contact, Φ is the potential barrier height at the corresponding contact expressed in units of eV, m^* is the effective mass of the electron or the hole , and h is Plank's constant.

The other set of boundary conditions corresponds to the HTL/AlQ_3 interface. A simple but rather approximate way to determine the boundary conditions of the electric field at this organic/organic heterojunction is to assume a constant electric displacement vector (εF) across the interface. In this case, the ratio of the electric field boundary conditions will be equal to the reciprocal ratio of the dielectric constants of the two materials on both side of the interface. However, this approximation assumes an ideal interface, and therefore ignores interface charges. A more accurate model, on the other hand, should account for the higher concentration of charges at the interface due to surface states, which would influence the electric field boundary condition. A model for the HTL/AlQ_3 interface should also address direct surface recombination between a hole on a HTL site and an electron on an AlQ_3 site. Clearly surface charges will have an dominant process in devices with a buffer layer or with a doped HTL due to the higher concentration of anionic AlQ_3 near the interface as discussed in section 5.2.

In order to address the effect of the hole-injection barrier at the HTL/AlQ_3 interface on OLED degradation, as discussed previously in chapter 5, the charge injection mechanism across the interface must be known. Unfortunately, phenomena at organic/organic heterojunctions are still not completely understood. In a recent study, models originally developed for inorganic semiconductor hereojunctions have been used to describe the HTL/AlQ_3 interface (Yang and Shen 1999-b, Lundstrom and Schuelke 1982). However, due to the much lower carrier concentrations and mobilities in organic solids, the applicability of this model to OLEDs is questionable.

Other boundary conditions can be determined from the total potential drop across the two layers which is equal to the sum of the potential drops across each layer and is related to the OLED driving voltage V by:

$$\int_{HTL} F\,dz \quad + \quad \int_{AlQ_3} F\,dz \quad = \quad V - V_{bi} \tag{6.18}$$

where V_{bi} is the built-in potential caused by the workfunction difference of the two electrodes.

6.2.3 The Case of an OLED with a Buffer Layer or a Dual-Layer HTL:

Similar to the case of a bilayer OLED, *F*, *n* and *p* profiles across an OLED with a buffer layer at the ITO/HTL interface or a dual-layer HTL can be obtained by modeling each of the three layers separately and then integrating them together through proper boundary conditions. In these devices, the buffer layer or the second hole transport layer can be modeled by a single-carrier (i.e. hole-only) current injection SCLC conduction, whereas the AlQ_3 layer is modeled by a double-carrier current injection SCLC conduction. The additional organic/organic heterojunction can be treated similar to the HTL/AlQ_3 interface.

6.2.4 The Case of an OLED with a doped HTL:

Doping the hole transport layer is known to partially shift the recombination zone to the HTL (Hamada *et al.* 1995). Such shift occurs because of the effectiveness of the dopant molecules in acting as hole traps, and therefore higher electron currents cross the interface from the AlQ_3 layer to the HTL to compensate for the lower hole currents in the opposite directions. Because the electron currents in the HTL are significant, their effect on the *F*, *n* and *p* profiles in the AlQ_3 can not be ignored as in the previous cases. Therefore, both the HTL and the AlQ_3 layer should be modeled by a double-carrier current injection SCLC conduction. In addition, because the dopant molecules act as trap sites in the HTL, their effect on modifying the profiles of trapped carriers p_t and n_t should be addressed.

6.3 Conclusion

In this chapter, some important aspects that must be addressed in a theoretical model to describe OLED degradation have been discussed. Following is a summary of the important features:

The spatial distribution profiles of electrons and holes across the organic layers of a device must be calculated using bipolar SCLC model. In this model, a field-dependent mobility should be used. Developing a solution for the governing equations of the SCLC model requires knowing boundary conditions at both the electrode/organic and organic/organic interfaces. Because quantum mechanical tunneling is the dominant injection process at the two electrode/organic interfaces, the boundary conditions at these interfaces could be obtained by using the Fowler-Nordheim equation. Calculating the boundary conditions at the HTL/AlQ_3 interface requires first having a model which describes charge injection across the organic/organic interface, which is still unavailable. Such interface model should also address the role of surface charges and direct recombination phenomena across the interface.

In order to calculate the rate of formation of Q species from AlQ_3^+ in an OLED, R_Q', both the electron-hole recombination rate, R_{eh} , and the rate of formation of Q species from AlQ_3^+ in the absence of recombination , R_Q , which both vary with position, must be first be determined. R_{eh} is calculated from the electron and hole distribution profiles using the Langevin model with a field-dependent mobility. However, a more realistic model should also include a field-dependent recombination rate according to the Onsager formalism. R_Q depends on the hole distribution profile across the AlQ_3 layer and on some reaction rate constant that can be determined experimentally.

Knowing R_Q' as a function of z, the spatial distribution of the Q species across the AlQ_3 layer, as a function of time, can then be calculated. The rate of decay of OLED luminance can then be calculated from the distribution of the Q species and from the magnitude of their effective radius, which, in turn, requires knowing their exciton quenching mechanism.

Obviously, modeling OLED degradation is a theoretical problem of significant complexity, and must address a number of fundamental phenomena that still are unclear or lack theoretical formalisms. Fortunately, some of these fundamental phenomena are currently the focus of recent studies (Anderson 1998, Yang and Shen 1999-b).

CHAPTER 7

Summary and Conclusions

Since efficient organic electroluminescence was reported in 1987, OLEDs have attracted special attention because of their potential toward the development of large-area flat panel displays. However, the relatively short operational lifetime of OLEDs has been the major problem preventing the commercialization of this technology. Degradation of OLEDs, macroscopically observed as a decay in the luminance with time, occurs due to the formation of microscopic non-luminous (dark) spots, and hence a reduction in the luminous area, as well as due to a decrease in the electroluminescence quantum efficiency of the luminous regions (intrinsic degradation). Although the processes leading to the formation of the dark spots had been identified and controlled, the causes of intrinsic degradation were unclear. Traditionally, intrinsic degradation has been speculated to be caused by morphological instability of the organic layers, especially the less stable hole transport layer, or by the formation of deep traps at the hole-injecting contact. These speculations were based on experimental observations showing that doping the organic layers or introducing a buffer layer at the hole-injecting contact can dramatically improve device stability. However, the real causes of OLED degradation remained uncertain, and therefore, the success of various stabilizing approaches, previously found by trial-and-error to improve OLED stability, remained limited to particular OLED material systems.

The objective of the research presented in this thesis is to explore and understand the aging phenomena that lead to the intrinsic degradation in OLEDs as a prerequisite for assigning effective measures to improve their stability. Understanding the aging processes is also necessary for developing a theory that addresses the degradation behavior, and hence in setting the design rules for the industrial production of OLEDs in the future.

In this study, the causes of the intrinsic long-term degradation of OLEDs based on tris(8-hydroxyquinolato) aluminum (AlQ_3), the most widely used electroluminescent molecule, are investigated. OLEDs of various structures are fabricated using physical vapor deposition in vacuum. These included standard bilayer devices, as well as ones utilizing previously reported stabilizing approaches (OLEDs with buffer layers at the hole injecting contact, and OLEDs with a doped HTL), and others with novel structures developed in this study (OLEDs with a mixed layer of electron and hole transport molecules). Following a control experiment approach, a systematic study to investigate both material and device aging phenomena resulting from operating these OLEDs is conducted. Material aging phenomena are studied by means of various characterization techniques capable of investigating thin films. These techniques include: optical and fluorescence microscopy (to study material morphology), atomic force microscopy (to study film topography), photoluminescence spectroscopy (to study energy bands and quantum efficiency), and infra-red absorption spectroscopy (to study material chemistry). OLED performance is studied by means of electrical dc measurements, such as, current density-voltage-luminance intensity (J-V-L) characterization (to study conduction and efficiency), lifetime measurements (to test stability), and electroluminescence spectroscopy (to study energy bands and recombination processes).

Contrary to what has been believed before, studies on OLEDs with a mixed layer reveal that degradation is not caused by morphological changes in the HTL or degradation at the anode/HTL interface, but rather near the HTL/AlQ_3 interface. Comparative studies on OLEDs with a buffer layer at the anode/HTL contact, OLEDs with a doped HTL, and bilayer standard OLEDs reveal that the role of the buffer layer or dopants in improving device stability is slowing the transport of holes to the AlQ_3 layer, suggesting that the injection of holes into the AlQ_3 layer is causing degradation. Further studies on AlQ_3 layers where only hole-currents or electron-currents are driven prove that degradation in OLEDs is indeed caused by the injection of holes into the AlQ_3 layer due to the formation of the unstable cationic AlQ_3 species and the production of fluorescence quenchers.

In view of these findings, the effectiveness of stabilizing agents, such as, doping the HTL, introducing a buffer layer at the hole-injecting contact, or using mixed layers of hole and electron transporting molecules, is explained in terms of their role in slowing down the injection of holes into the AlQ_3, which results in a higher electron density and thus a more rapid electron-hole recombination. Therefore, the lifetime of the unstable cationic AlQ_3 species is reduced leading to a significant decrease in AlQ_3 degradation and consequently increases device stability. Under the most favorable conditions, the cationic AlQ_3 species may not be formed at all as holes could be injected into anionic AlQ_3 species producing excited states directly, without the formation of cationic intermediates. Other earlier observations pertaining to OLED degradation are also explained in terms of the same mechanism. For instance, the correlation between a higher ionization potential of the hole transport material and a higher OLED stability is explained in terms of the higher hole injection barrier at the HTL/AlQ_3 interface, and hence less AlQ_3 degradation. The correlation between a lower cathode work function and a higher OLED stability is explained in terms of the easier injection of electrons into the AlQ_3 layer that leads to a higher electron density near the HTL/AlQ_3 interface, and hence a rapid electron hole recombination.

The degradation mechanism is further demonstrated using OLEDs with dual-layer HTL made of materials with different ionization potentials. When the order of the two layers is in such a way so as to facilitate the transport of holes to the AlQ_3 layer via energy cascading, the OLEDs show poor stability. On the other hand, switching the order of the two hole transport layers leads to the formation of higher hole injection barriers and results in a remarkable increase in device stability. This effect not only confirms the role of the injection of holes into the AlQ_3 layer on device degradation, but also demonstrates novel approaches to improve OLED stability.

Finally, important aspects that must be addressed in a theoretical model to describe OLED degradation are discussed. In this discussion, the factors governing the degradation kinetics are presented. A general theoretical background of space-charge-limited-current conduction model, needed to calculate the electron and hole concentration profiles, is also provided. A number of particularly important OLED structures; standard bilayer devices, OLEDs with a buffer layer or dual-layer HTL, and OLEDs with a doped HTL, are addressed.

REFERENCES

1. Adachi, C., Nagai, K., Tamoto, N., 1995, *Appl. Phys. Lett.*, **66**, 2679.

2. Anderson, J.D., McDonald, E.M., Lee, P.A., Anderson, M.L., Ritchie, E.L., Hall, H.K., Hopkins, T., Mash, E.A., Wang, J., Padias, A., Thayumanavan, S., Barlow, S., Marder, S.R.,Jabbour, G.E., Shaheen S., Kippelen, B., Peyghambarian, N., Wightman R.M., Armstrong, N.R., 1998, *J. Am. Chem. Soc.*, **120**, 9646.

3. Arai, M., Nakaya, K., Onitsuka, O., Inoue, T., Codama, M., Tanaka, M., Tanabe, H., 1997, *Synth. Met.*, **91**, 21.

4. Aziz, H., Xu, G., 1996, *Synth. Met.*, **80**, 7.

5. Aziz , H., Xu, G., 1997, *J. Phys. Chem. B*, **101**, 4009.

6. Aziz,H., Popovic, Z.D., Xie, S., Hor, A., Hu, N., Tripp, C.,Xu, G., 1998-a, *Appl.Phys. Lett.*, **72**, 756.

7. Aziz,H., Popovic, Z.D., Tripp, C.P., Hu, N., Hor, A., Hu, N., Tripp, C., Xu, G., 1998-b, *Appl.Phys. Lett.*, **72**, 2642.

8. Aziz, H., Popovic, Z.D., Hu, N., Hor, A., Xu, G., 1999-a, *Science*, **283**, 1900.

9. Aziz, H., Popovic, Z.D., Hu, N., Hor, A., Xu, G., 1999-b, in *Proceedings of the MRS Spring Meeting*, San Francisco, CA, April 1999, (submitted for publication)

10. Barltrop, J.A., Coyle, J.D., Principles of Photochemistry. John Wiley and Sons Ltd.,1978.

11. Bin, L.B., Jenekhe, S.A., Young, R.H., Borsenberger, P.M., 1997, *Appl. Phys. Lett.*,**70**, 2052.

12. Borsenberger, P.M., Weiss, D.S. Organic Photoreceptors for Photography. Marcel Dekker, Inc., 1998.

13. Bulovic, V., The Role of Excitons and Interfaces in Molecular Organic Devices. Ph.D. Thesis. Princeton University, 1998.

14. Burrows, P.E., Forrest, S.R., 1994, *Appl. Phys. Lett.*, **64**, 2285.

15. Burrows, P.E., Bulovic, V., Forrest, S.R., Sapochak, L.S., McCarty, D.M.,Thompson, M.E., 1994, *Appl. Phys. Lett*, **65**, 2922.

16. Burrows, P.E., Shen, Z., Bulovic, V., McCarty, D.M., Forrest, S.R., Cronin, J.A., Thompson, M.E., 1996, *J. Appl. Phys.*, **79**, 7991.

17. Campbell, I.H., Davids, P.S., Smith, D.L., 1998, *Appl. Phys. Lett.*, **72**, 1863.

18. Campbell, I.H., Smith, D.L., 1999, *Appl. Phys. Lett.*, **74**, 561.

19. Cowie, J.M.G. Polymers: Chemistry and Physics of Modern Materials. 2nd ed., Balckie Academic, London, 1991.

20. Do, L.M., Han, E.M., Niidome, Y., Fujihira, M., Kanno, T., Yoshida, S., Maeda, A., Ikushima, A.J., 1994, *J. Appl. Phys.*, **76**, 5118.

21. Do, L.M., Oyamada, M., Koike, A., Han, E.M., Yamamoto, N., Fujihira, M., 1996-a, *Thin Solid Films*, **273**, 209.

22. Do, L.M., Han, E.M., Yamamoto, M., 1996-b, *Mol. Cryst. Liq. Cryst.*, **280**, 373.

23. Dresner, I., 1969, *RCA Review.*, **30**, 322.

24. Forsythe, E.W., Morton, D.C., Tang, C.W., Gao, Y., 1998, *Appl. Phys. Lett.*, **73**, 1457.

25. Fowler, R.H., Nordheim, N., 1928, *Proc. R.. Soc. London Ser. A*, **119**, 173.

26. Fujihira, M., Do, L., Koike, A., Han, E., 1996, *Appl. Phys. Lett.*, **68**, 1787.

27. Gutmann, F., Lyons, L.E. Organic Semiconductors. John Wiley & Sons, Inc.,1967.

28. Han, E.M., Do, L.M., Niidome, Y., Fujihira, M., 1994 , *Chem. Lett.*, 969.

29. Han, E.M., Do, L.M., Yamamoto, N., Y., Fujihira, M., 1995-a, *Mol. Cryst. Liq. Cryst.*, **267**, 411.

30. Han, E.M., Do, L.M., Yamamoto, N., Fujihira, M., 1995-b , *Chem. Lett.*, 57.

31. Han, E.M., Do, L.M., Yamamoto, N., Fujihira, M., 1996, *Thin Solid Films*, **273**, 202.

32. Hamada, Y., Sano, T., Shibata, K., Kuroki, K., 1995, *Jpn. J. Appl. Phys.*, **34**, L824.

33. Haskal, E.I., 1997, *synth. Met.*, **91**, 187.

34. Hosokawa, C., Matsuura, M., Eida, M., Hironaka, Y., Kusumoto, T., 1996, *IS&T's 49th Annual Conference*, 388.

35. Ioannidis, A., Forsythe, E., Gao, Y., Wu, M.W., Conwell, E.M., 1998, *Appl. Phys. Lett.*, **72**, 3038.

36. Itano, K., Tsuzuki, T., Ogawa, H., Appleyard, S., Willis, M., Shirota, Y., 1997, *IEEE Transactions on Electron Devices*, **44**, 1218.

37. Jabbour, G.E., Kawabe,S.E., Shaheen, S.E., Wang, J.F., Morrell, M.M., Kippelen, B., Peyghambarian,N., 1997, *Appl. Phys. Lett.*, **71**, 1762.

38. Kalinowski, J., Di Marco, P., Camaioni, N., Fattori, V., Stampor, W., Duff, J., 1996-a, *Synth. Met.*, **76**, 77.

39. Kalinowski, J., Camaioni, N., Di Marco, P., Fattori, V., Giro, G., 1996-b, *Int. J. Electronics*, **81**, 377.

40. Kao, K.C., Hwang, W. Electrical Transport in Solids; with Particular Reference to Organic Semiconductors. Pergamon Press, 1981. (In Canada: Pergamon of Canada, Willodale, Ontario.)

41. Kawabe, Y., Morrell, M.M., Jabbour, G.E., Shaheen S.E., Kippelen, B., Peyghambarian, N., 1998, *J. Appl. Phys.*, **84**, 5306.

42. Kawaharda, M., Ooishi, M., Saito, T., Hasegawa, E., 1997, *Synth. Met.*, **91**, 113.

43. Kido, J., Kimura, M., Nagai, K., 1995, *Science*, **267**, 1332.

44. Kido, J., Iizumi, Y., 1998, *Appl. Phys. Lett.* **73**, 2721.

45. Kido, J., Kohda, M., Okuyama, K., Nagai, K., 1992, *Appl. Phys. Lett.*, **61**, 761.

46. Lundstrom, M.S., Schuelke, R.J., 1982, *Solid State Electronics*, **25**, 683.

47. Malliaras, G.G., Scott, J.C., 1998, *J. Appl. Phys.* **83**, 5399.

48. Matsumura, M., Jinde, Y., 1997, *Synth. Met.*, **91**, 197.

49. McElvain, J., Antoniadis, H., Hueschen, M.R., Miller, J.N., Roitman, D.M., Sheets J.R., Moon, R.L., 1996, *J.Appl.Phys.*, **80**, 6002.

50. Mori, T., Miyachi, K., Kichimi, T., Mizutani, T., 1994, *Jpn. J. Appl. Phys.*,**33**, 6594.

51. Mori, T., Miyake, S., Mizutani, T., 1995, *Jpn. J. Appl. Phys.*, **34**, 4120.

52. Mori, T., Obata, K., Miyachi, K., Mizutani, T., Kawakami, Y., 1997, *Jpn. J. Appl. Phys.*, **36**, 7240.

53. Murata, H., Merritt, c.D., Kafafi, Z.H., 1998, *IEEE Journal of Selected Topics in Quantum Electronics*, **4**, 119.

54. Naka, S., Shinno, K., Okada, H., Onnagawa, H., Miyashita, K., 1994, *Jpn. J. Appl. Phys.*, **33**, L1772.

55. Okutusu, S., Onikubo, T., Tamano, M., Enokida, T., 1997, *IEEE Transactions on Electron Devices*, **44**,1302.

56. Papadimitrakopoulos, F., Zhang, X.-M., Thomsen, D.L., III, Higginson, K.A.,1996,*Chem.Mater.* **8**, 1363.

57. Pope,M., Kallmann, H.P., Magnatte, P., 1963, *J. Chem. Phys.*, **38**, 2042.

58. Pope, M., Swenberg, C.E. Electronic Processes in Organic Crystals. Oxford University Press, 1982.

59. Popovic, Z.D., Aziz, H., Tripp, C.P., Hu, N.,, Hor, A., Xu, G., 1998, in *Proceedings of the SPIE*, Volume 3476, *Organic Light-Emitting Materials and Devices II*, San Diego, CA, July 1998, pp 68-73.

60. Salbeck, J., 1996, *Ber. Bunsenges. Phys. Chem.*, **100**, 1667.

61. Sato, Y., Kanai, H., 1994, *Mol. Cryst. Liq. Cryst.*, **253**, 143.

62. Sato, Y., Ogata, T., Ichinosawa, S., Murata, Y., 1997, *Synth. Met.*, **91**, 103.

63. Scott, J.C., Karg, S., Carter, S.A., 1997, *J. Appl. Phys.*, **82**, 1454.

64. Sheats, J.R., Antoniadis, H., Hueschen, M., Leonard, W., Miller, J., Moon, R., Roitman, D., Stocking, A., 1996, *Science*, **273**, 884.

65. Shen, Z., Burrows, P.E., Bulovic, V., Forrest, S.R., Thompson, M.E., 1997, *Science,* **276**, 2009Shi, J., Tang, C.W., 1997, *Appl. Phys. Lett.* **70**, 1665.

66. Shen, J., Yang, J., 1998, *J. Appl. Phys.,* **83**, 7706.

67. Shen, J., personal communication, May 1999.

68. Shi, J., Tang, C.W., 1997, *Appl. Phys. Lett.,***70**, 1665.

69. Shirota, Y., Kuwabara, Y., Inada, H., Wakimoto, T., Nakada, H., Yonemoto, Y., Kawami, S., Imai, K., 1994, *Appl. Phys. Lett.,* **65**, 807.

70. Shirota, Y., Kuwabara, Y., Okuda, D., Okuda, R., Ogawa, H., Inada, H., Wakimoto, T., Nakada, H., Yonemoto, Y., Kawami, S., Imai, K., 1997, *J.Luminescence,* **72-74**, 985.

71. Sokolik, I., Priestley, R., Walser, A.D., Dorsinville, R., Tang, C.W., 1996, *Appl. Phys. Lett.,* **69**, 4168.

72. Tanaka, H., Tokito, S., Taga, Y., Okada. A., 1996, *Chem. Commun.,* 2175.

73. Tang, C.W., VanSlyke, S.A., 1987, *Appl. Phys. Lett.,* **51**, 913.

74. Tang, C.W., Van Slyke, S.A., Chen, C.H., 1989, *Appl. Phys. Lett.,* **65**, 3610.

75. Tessler, N., Harrison, N.T., Thomas, D.S., Friend, R.H., 1998, *Appl. Phys. Lett.,* **73**, 732.

76. Van Slyke, S.A., Chen, C.H., Tang, C.W., 1996, *Appl. Phys. Lett.,* **69**, 2160.

77. Vestweber, H., Rieb, W., 1997, *Synth. Met.,* **91**, 181.

78. Wakimoto, T., Fukada, Y., Nagayama, K., Yokoi, A., Nakada, H., Tsuchida, M., 1997-a, *IEEE Transactions on Electron Device,* **44**, 1245.

79. Wakimoto, T., Yonemoto, Y., Funaki, J., Tsuchida, M., Murayama, R., Nakada, H., Matsumoto, H., Yamamura, S., Nomura, M., 1997-b, *Synth. Met.,* **91**, 15.

80. Wilson, J. Optoelectronics: An Introduction. Prentice-Hall International Inc., 1983.

81. Wu, C.-C., Sturm, J.C., Register, R.A., Tian, J., Dana, E.P., Thompson, M.E., 1997, *IEEE Transactions on Electron Devices,* **44**, 1269.

82. Yang, J., Shen, J., 1998, *J. Appl. Phys.,* **84**, 2105.

83. Yang, J., Shen, J., 1999-a, *J. Appl. Phys.,* **85**, 2699.

84. Yang, J., Shen, J., 1999-b, *Appl. Phys. Lett.*, (submitted for publication).

85. Young, R.H., 1994, *Phil. Mag. Lett*, **70**, 331.

86. Zhang, Z., Jiang, X., Xu, S., Nagatomo, T., Omoto, O., 1997, *Synth. Met.*, **91**, 131.

87. Zhang, Z., Jiang, X., Xu, S., Nagamoto, T., Omoto, O., 1998, *J. Phys. D: Appl. Phys.*, **31**, 32.